



LUND UNIVERSITY

SOFC Modeling Considering Mass and Heat Transfer, Fluid Flow with Internal Reforming Reactions

Andersson, Martin

DOI:

[10.13140/RG.2.2.15303.09122](https://doi.org/10.13140/RG.2.2.15303.09122)

2009

[Link to publication](#)

Citation for published version (APA):

Andersson, M. (2009). *SOFC Modeling Considering Mass and Heat Transfer, Fluid Flow with Internal Reforming Reactions*. [Licentiate Thesis, Faculty of Engineering, LTH]. <https://doi.org/10.13140/RG.2.2.15303.09122>

Total number of authors:

1

General rights

Unless other specific re-use rights are stated the following general rights apply:

Copyright and moral rights for the publications made accessible in the public portal are retained by the authors and/or other copyright owners and it is a condition of accessing publications that users recognise and abide by the legal requirements associated with these rights.

- Users may download and print one copy of any publication from the public portal for the purpose of private study or research.
- You may not further distribute the material or use it for any profit-making activity or commercial gain
- You may freely distribute the URL identifying the publication in the public portal

Read more about Creative commons licenses: <https://creativecommons.org/licenses/>

Take down policy

If you believe that this document breaches copyright please contact us providing details, and we will remove access to the work immediately and investigate your claim.

LUND UNIVERSITY

PO Box 117
221 00 Lund
+46 46-222 00 00



LUNDS UNIVERSITET
Lunds Tekniska Högskola

SOFC Modeling Considering Mass and Heat Transfer, Fluid Flow with Internal Reforming Reactions

Karl **Martin** Johan **Andersson**

Thesis for the degree of Licentiate of Engineering, 2009

Division of Heat Transfer
Department of Energy Sciences
Faculty of Engineering (LTH)
Lund University

www.energy.lth.se

Copyright © Karl Martin Johan Andersson, 2009
Division of Heat Transfer
Department of Energy Sciences
Faculty of Engineering (LTH)
Lund University
Box 118, SE-221 00, Lund, Sweden

ISRN LUTMDN/TMHP--09/7063--SE
ISSN 0282-1990

Abstract

Fuel cells are promising for future energy systems, since they are energy efficient and, when hydrogen is used as fuel, there are no emissions of greenhouse gases. Fuel cells have during recent years various improvements, however the technology is still in the early phases of development. This can be noted by the lack of a dominant design both for single fuel cells, stacks and for entire fuel cell systems.

A literature study is performed to compile the current position in fuel cell modeling. A deeper investigation is made to find out if it is possible to use a multiscale approach to model solid oxide fuel cells (SOFCs) and combine the accuracy at microscale with for example the calculation speed at macroscale to design SOFCs, based on a clear understanding of transport phenomena and functional requirements. It is studied what methods can be used to model SOFCs and also to sort these models after length scale. Couplings between different methods and length scales, i.e., multiscale modeling, are outlined. Multiscale modeling increases the understanding for detailed transport phenomena, and can be used to make a correct decision on the specific design and control of operating conditions. It is expected that the development and production costs will decrease and the energy efficiency increase (reducing running cost) as the understanding of complex physical phenomena increases.

In this thesis a CFD approach (COMSOL Multiphysics) is employed to investigate the effects on the temperature distribution from inlet temperature, oxygen surplus, ionic conductivity and current density for an anode-supported intermediate temperature solid oxide fuel cell (IT-SOFC). The developed model is based on the governing equations of heat-, mass- and momentum transport. A local temperature non-equilibrium (LTNE) approach is introduced to calculate the temperature distribution in the gas- and solid phase separately. This basic model is extended to include internal reforming reactions and effects on mass- and heat transfer, and on fluid dynamics.

The results show that the temperature increase along the flow direction is controlled by the degree of surplus air. It is also found that the ohmic polarization in the electrolyte and the activation polarization in the anode and the cathode have major influence on the heat generation and cell efficiency. If a counter flow approach is employed the inlet temperature for the fuel stream should be close to the outlet temperature for the air flow to avoid a too high temperature gradient close to the fuel inlet. The temperature is lowered, when hydrocarbon fuels (e.g., methane) is used, due to the reforming reactions.

Keywords: IT-SOFC, modeling, CFD, LTNE, COMSOL Multiphysics, transport phenomena, internal reforming reaction, catalyst

Populärvetenskaplig beskrivning på svenska

Bränslecellen uppfanns redan 1838, det kommersiella genombrottet dröjde till 2007, den framtida potentialen är mycket lovande

Domedagsprofetior angående växthuseffektens betydelse för livet på jorden når oss via media allt oftare. Bränsleceller är mycket lovande för ett framtida miljövänligt samhälle. Hög energieffektivitet och inga utsläpp av koldioxid, kväveoxider eller hälsoskadliga partiklar är några av fördelarna. Ett minskat behov av olja kan leda till ett minskat beroende av oberäkneliga oljestater och på sikt till en fredligare värld.

Bränslecellens utveckling

Bränslecellen är ingen ny uppfinning, idén upptäcktes av Christian Friedrich Schönbein år 1838. Han var en tysk-schweizisk kemist, som var verksam vid universitet i Basel. Det dröjde fram till 1950-talet innan kompletta bränslecellssystem var konstruerade. Anledningen till att utvecklingen var långsam till en början kan till stor del förklaras med tillgången till billig olja. Bränsleceller blev mer allmänt kända då de användes som kraftkälla i det amerikanska rymdprogrammet Apollo. Forskningen har ökat mycket under senare år på grund av ökade bränslepriser och diskussionen kring växthuseffektens påverkan på jordens klimat.

Hur fungerar en bränslecell?

Den enklaste formen av en bränslecell bygger på att syre och väte reagerar med varandra och bildar vatten. En bränslecell är uppbyggd av en anod, en katod och en elektrolyt. En anod är den del i en elektrolytisk cell som är förbunden med strömkällans positiva pol, och katoden är sammanbunden med dess negativa pol. Elektrolyten kan liknas vid ett membran. Det gasformiga bränslet transporteras till anoden där det reagerar i elektrokemiska reaktioner med syrejoner. Syrejonerna produceras i katoden där syre reagerar med elektroner till jonform. Syrejonerna transporteras igenom elektrolyten för att nå bränslet i anoden. Elektronerna släpps inte igenom elektrolyten, vilket gör att en spänning uppstår.

Den givna beskrivningen gäller för vad som sker i en fastoxidbränslecell, men också övriga typer av bränsleceller är uppbyggda av motsvarande principer. Fastoxidbränsleceller har en hög arbetstemperatur, elektrolyten, bestående av en fastoxid, är utformad för att endast släppa igenom syrejoner som transporteras från katoden till anoden. Skillnaden mellan olika typer av bränsleceller är främst vilken typ av elektrolyt som används och bränslecellens arbetstemperatur.

Bränsleceller producerar elektricitet och värme direkt från kemiska reaktioner mellan bränsle och luft. Vilket bränsle som kan användas beror på vilken typ av bränslecell. När ren vätgas eller biogas används blir det inga nettoutsläpp av koldioxid, hälsoskadliga partiklar eller kväveoxider. Processen är på så sätt helt miljövänlig och koldioxidneutral.

Liten som en ärtä till stor som ett kraftverk

Den framtida potentialen för bränsleceller är mycket stor eftersom de kan byggas i många olika storlekar. Mycket små för att ersätta ett batteri, små för att generera el till kringutrustning i en bil eller lastbil, stora för att ersätta motorn i en personbil och mycket stora i form av ett kraftvärmeverk. De största hindren för en kommersialisering i stor skala är tillverkningskostnaden, livslängden och saknaden av en infrastruktur för vätgas och biogas/naturgas.

Fred på jorden?

En ökad användning av bränsleceller kan leda till en ökad lokal bränsleproduktion, och därmed ett minskat beroende från import av olja och naturgas från länder där politisk instabilitet hör till vardagen. Dispyter angående rättigheter till oljeproduktion har resulterat i flera krig på senare år som kriget mellan Iran och Irak, Kuwaitkriget och Irakkriget. En ökad användning av effektiva energisystem, där bränsleceller är en viktig nyckelkomponent, kan vara viktigt för skapandet av en fredligare värld.

Den egna forskningen

För fastoxidbränsleceller där arbetstemperaturen är mellan 600 och 800 °C är det möjligt att använda sig av mer komplexa bränslen jämfört med vätgas, som naturgas, biogas eller diesel. Då sker en omvandling av bränslet, antingen i en egen enhet som bränslet får passera innan det kommer till bränslecellen, eller inne i bränslecellens anod. Det material som vanligtvis används i anoden har visat sig vara lämpligt för katalytisk omvandling av naturgas och biogas till vätgas och kolmonoxid, vilka kan användas som bränsle i de elektrokemiska reaktionerna med syrejoner som sker i bränslecellens anod.

Forskningen inom forskargruppen i Lund har visat på fördelar med att omvandla biogas eller naturgas inne i bränslecellen. Värme som kommer från de elektrokemiska reaktionerna kan användas inne i bränslecellen för att driva omvandlingen av biogas till vätgas och kolmonoxid. Den totala effektiviteten ökar samtidigt som de totala temperaturskillnaderna minskar. Resultaten kan på sikt leda till en minskad produktionskostnad och en ökad livslängd.

Hur långt har utvecklingen kommit?

Bränsleceller anses vara i kommersiell tillverkning från och med år 2007. Produktion i stor skala har startat för ett antal nischmarknader inom rymdprogrammen, för militära ändamål och som reservkraft för till exempel sjukhus eller mobilmaster. Inom några år kommer sannolikt bränslecellssystem att vara mer vanliga inom fordonsindustrin. Det är en enorm marknad som hägrar. En ökad forskning och utveckling på bränsleceller kommer att leda till en ökad ekonomisk tillväxt.

Framtida möjligheter

Volvo lastvagnar är bland de ledande i forskningen och de hoppas kunna introducera ett bränslecellssystem på marknaden år 2011. Det kan nämnas att Toyota förväntar sig en dubblad verkningsgrad om bränsleceller ersätter dagens förbränningsmotorer i bilar. En världsmarknad för bränsleceller på 120 miljarder kronor förväntas redan år 2013, och därefter kraftigt växande, i takt med att tillverkningskostnaden minskar, verkningsgraden och livslängden ökar. De största konkurrenterna till bränsleceller är ett lågt pris på olja samt bristen på ett väl utvecklat system för säker lagring av ett gasformigt fordonsbränsle.

I takt med att tillverkningskostnaderna sjunker och/eller bränslepriserna stiger ökar antalet områden där bränsleceller blir mer prisvärda jämfört med nuvarande teknologier så som batterier, motorer eller kraftverk. Den internationella energimyndigheten (IEA) förutspår att vätgas motsvarande 15 procent av dagens råoljeproduktion kommer att användas i bränsleceller för fordon år 2050. IEA förutspår vidare en installerad effekt motsvarande mer än den nuvarande effekten från kärnkraft i hela världen för stationära bränslecellssystem år 2050. För att uppnå denna stora betydelse måste tillverkningskostnaden sjunka och livslängden öka.

Sammanfattningsvis

Problemen och utmaningarna med dagens energisystem är både globala och lokala med utsläpp av bland annat koldioxid, hälsoskadliga partiklar och kväveoxider. Man vet att det finns en begränsad mängd av fossila bränslen och det diskuteras hur länge mänskligheten kan fortsätta att utvinna olja i samma takt som idag. Möjligheten av en ren, miljövänlig och energieffektiv bränsleanvändning driver utvecklingen av bränsleceller och bränslecellssystem framåt i ett allt snabbare tempo. Det som kommer att bestämma tillväxten inom bränslecellsområdet är hur snabbt tillverkningskostnaden kan sänkas, livslängden ökas samt utvecklingen av oljepriset.

Den aktuella forskningen är finansierad av den svenska staten via Vetenskapsrådet.

Acknowledgements

This work has been carried out at the Division of Heat Transfer, Department of Energy Sciences, Lund University, Sweden.

I would like to express great appreciation to my supervisors Docent Jinliang Yuan and Professor Bengt Sundén, for allowing me a lot of freedom in my work, many discussions and a lot of support and guidance during the last two years.

My deep appreciation goes to all my fellow PhD students at the Division of Heat Transfer for interesting discussions, cooperation and support during the last two years.

Many thanks go to my family and friends for all encouragement and support.

The current work is financially supported by the Swedish Research Council (Vetenskapsrådet, VR).

List of publications

Publications included in this thesis:

1. **M. Andersson**, J. Yuan, B. Sundén, *Chemical reacting transport phenomena and multiscale models for SOFCs*, in: Proceedings of Heat Transfer, Maribor, Slovenia, WIT Press, UK, June 2008
2. **M. Andersson**, J. Yuan, B. Sundén, W. G. Wang, *LTNE approach and simulation for anode-supported SOFCs*, ASME FuelCell2009-85054, to appear in: Proceedings of the 7th International Fuel Cell Science, Engineering & Technology Conference, Newport Beach, California, USA, June 2009

Publications not included in this thesis:

1. J. Yuan, G. Yang, **M. Andersson**, B. Sundén, *Analysis of chemical reacting heat transfer in SOFCs*, in: Proceedings of 5th European Thermal Sciences Conference, Eindhoven, Netherlands, 2008
2. J. Yuan, G. Yang, **M. Andersson**, B. Sundén, *CFD approach for chemical reaction coupled heat transfer in SOFC channels*, in: Proceedings of 7th International Symposium on Heat Transfer, ISHT7, Beijing, China, 2008

Table of contents

Abstract.....	i
Populärvetenskaplig beskrivning på svenska	ii
Acknowledgements	iv
List of publications	v
Table of contents	vi
Nomenclature	viii
1 Introduction.....	1
1.1 Background.....	1
1.2 Objectives	1
1.3 Methodology.....	2
1.4 Outline of the thesis	2
2 Literature survey and problem statement.....	3
2.1 Introduction to fuel cells	3
2.1.1 Historical development	4
2.1.2 Future fuel cell potential	4
2.2 Various types of fuel cells.....	6
2.3 Solid Oxide Fuel Cells (SOFCs).....	7
2.4 SOFC modeling development	8
2.4.1 Micro-, meso- and macroscale approaches.....	9
2.4.2 SOFC modeling at microscale.....	10
2.4.3 SOFC modeling at mesoscale.....	10
2.4.4 SOFC modeling at macroscale	11
2.4.5 SOFC modeling integration issues	11
2.5 Transport processes	12
2.5.1 Mass transport	12
2.5.2 Momentum transport	13
2.5.3 Heat transport.....	14
2.5.4 Integration issues.....	14
2.6 Electrochemical reactions	14
2.7 Internal reforming reactions	15
2.7.1 Surface chemistry	16
2.7.2 Global kinetics	17
3 Mathematical models	19
3.1 Assumptions.....	20
3.2 Governing equations	21
3.2.1 Momentum equation	21
3.2.2 Mass transport equation.....	21
3.2.3 Heat transfer equation.....	23
3.3 Boundary and interface conditions	25
3.3.1 Momentum transport	25
3.3.2 Mass transport	25
3.3.3 Heat transfer	26
3.5 Extended model considering internal reforming reactions.....	28
3.6 Numerical methods	31

4 Results.....	32
4.1 Basic model.....	32
4.2 Model considering internal reforming reactions.....	38
5 Conclusions	43
6 Future work.....	44
7 References	45

Nomenclature

\dot{n}	molar flux, mol/(m ² ·s)
C	fuel consumption, dimensionless
d_c	channel diameter, m
c_p	specific heat capacity at constant pressure, J/(kg·K)
Da	Darcy number, dimensionless
D_{ii_T}	Maxwell-Stefan binary diffusion coefficient, m ² /s
D_i	thermal diffusion coefficient, kg/(m·s)
d_p	electrode particle diameter, m
E	activation energy, kJ/mol
e	characteristic Lennard-Jones energy, K
\mathbf{F}	volume force vector, N/m ³
F	Faraday constant, 96485 C/mol
h	enthalpy, kJ/mol
h_{sg}	heat transfer coefficient, W/(m ² ·K)
h_v	volume heat transfer coefficient, W/(m ³ ·K)
i	current density, A/cm ²
i_0	exchange current density, A/cm ²
k	thermal conductivity, W/(m·K)
k_i	reaction rate constant, mol/(m ³ ·Pa ² ·s)
k'	Boltzmann's constant, J/K
k''	pre-exponential factor, 1/(Ω·m ²)
K_e	equilibrium constant, Pa ² or dimensionless
l_{ij}	characteristic length, Å
M	molecular weight the mixture, kg/mol
M_j	molecular weight of species j, kg/mol
n_0	inlet mass flux, kg/(m ² ·s)
n_e	number of electrons transferred per reaction, -
Nu	Nusselt number, dimensionless
p	pressure, Pa, bar
q	heat flux, W/m ²
Q	source term (heat), W/m ³
r	velocity effect due to electrochemical reaction, m/s
r_i	chemical reaction rate, mol/(m ³ ·s), mol/(m ² ·s), mol/(m·s)
\bar{r}	average pore radius, m
R	gas constant, 8.314 J/(mol·K)
R_{ohm}	electrolyte area-specific ohmic resistance, Ω/m ²
S	air surplus factor, dimensionless
S_i	reaction rate, kg/(m ³ ·s)
SA	surface area, m ² /m ³
ΔS_r	entropy change of reaction, J/(K·mol)
T	temperature, K
\mathbf{T}	viscous stress tensor, N/m ²
t	tortuosity, dimensionless
u, v	velocity, m/s
w_i	mass fraction of species i, kg/kg
x, y	coordinate system, m
x_j	molar fraction of species j, mol/mol

Greek symbols

ε	porosity, dimensionless
η	over potential, V
κ	permeability, m ²
κ_{dv}	deviation from thermodynamic equilibrium, Pa·s
μ	dynamic viscosity, Pa·s
ρ	density, kg/m ³
σ	ionic/electronic conductivity, $\Omega^{-1}\text{m}^{-1}$
τ	component thickness, m
Ω_D	diffusion collision integral, dimensionless

Subscripts

0	initial
a	anode
act	activation polarization
b	bulk
c	cathode
conc	concentration polarization
e	electrode, $e \in \{a, c\}$
el	electrolyte
f	fluid phase
g	gas phase
i	molecule i
int	interconnect
j	molecule j
K	Knudsen diffusion
losses	activation and concentration polarization
ohm	ohmic polarization
r	steam reforming reaction
por	porous media
s	solid phase, water-gas shift reaction
w	gas channel wall
+	forward reaction
-	reverse reaction

Abbreviations

AFC	alkaline fuel cell
APU	auxiliary power unite
CFD	computational fluid dynamics
DFT	density functional theory
DGM	dusty gas model
DMFC	direct methanol fuel cell
FC	fuel cell
FEM	finite element method
FM	Fick's model
FVM	finite volume method
IEA	International Energy Agency
IT	intermediate temperature
KMC	kinetic Monte Carlo
LBM	lattice Boltzmann method
LHV	lower heating value
LSM	strontium doped lanthanum manganite
LTE	local temperature equilibrium
LTNE	local temperature non-equilibrium
MD	molecular dynamics

MCFC	molten carbonate fuel cell
PAFC	phosphoric acid fuel cell
PEMFC	polymer electrolyte membrane fuel cell
SA	surface area
SC	steam-to-carbon ratio
SMM	Stefan-Maxwell model
SOFC	solid oxide fuel cell
TPB	three-phase boundary
YSZ	yttria-stabilized zirconia

Chemical

CH ₄	methane
CO	carbon monoxide
CO ₂	carbon dioxide
H ₂	hydrogen
H ₂ O	water
H ₂ S	hydrogen sulfide
N ₂	nitrogen
Ni	nickel
O ₂	oxygen
S	sulphur

Chapter 1

Introduction

This work is based on a research project supported by the Swedish Research Council (Vetenskapsrådet). It contains modeling and analysis of heat-, mass transfer, fluid flow and (electro-) chemical reactions inside intermediate temperature anode supported SOFCs. A basic model that uses a hydrogen/steam mixture as fuel is first developed, and further extended to include internal reforming reactions of hydrocarbon fuels as well.

1.1 Background

The future fuel cell potential is enormous, however the production cost must be decreased and the life time increased before becoming an important part in the energy system. There is a need for multi-physics multiscale SOFC models, as most models in the literature do not consider mass-, heat-, momentum transport and chemical reactions simultaneously. Strong coupling between the mentioned phenomena makes multi-physics SOFC modeling promising for optimizing the design and decreasing the production cost. The mass transport depends on material structure in the porous electrodes, the chemical reactions, the temperature distribution and the species concentrations. The fluid flow depends on the chemical reactions, temperature and fluid characteristics. The heat transport depends on the polarization losses, the chemical reactions, the fluid flow and the material structure. The reforming reactions depend on temperature, concentration and amount of catalyst available.

Research on the physical phenomena can be divided in different levels of scale. Microscale corresponds to atom or molecular level, macroscale corresponds to the global flow field. The macroscale transport phenomena are depending on the reforming surface chemical reactions, occurring on the particle surface (microscale). The ohmic polarization (depending on microscale parameters) within the electrolyte causes a significant part of the overall heat generation (macroscale).

It has been concluded in this thesis that most of the heat losses within the cells are generated due to ionic resistance in the electrolyte and activation polarization in the electrodes. The knowledge related to these phenomena is expected to increase when the developed model is further extended to include microscale phenomena within the electrodes and electrolyte. The methane reforming reaction depends on the microscale- catalyst distribution and mass transport, and a steep temperature gradient caused by the internal reforming reactions can lead to a decreased life time of the cells.

1.2 Objectives

The overall aim of this study is to analyze heat-, mass transport and fluid flow in solid oxide fuel cells, in order to increase the understanding of complex physical phenomena occurring inside SOFCs, and to increase the efficiency and decrease the production cost. A model should be developed to enable prediction of concentration- and temperature distributions. The objectives may be formulated in more details as given below:

- Through literature studies, the state-of-the-art CFD modeling has been reviewed including heat-, mass-, momentum transport and internal reforming reactions within

SOFCs. Modeling concerning physical phenomena at different scales and the integration between the different scales are identified.

- To identify where the most significant heat losses occur, to be able to increase the efficiency with more suitable design.
- To investigate the effect of the internal reforming reactions on the temperature and the concentrations.

1.3 Methodology

A literature review is conducted to find out what methods have been developed to model SOFCs, arranged according to length scales. Coupling between different methods and length scales, i.e., multiscale modeling, is outlined. SOFC microscale models correspond in many cases to the atom or molecular level. The Finite Element Method and Finite Volume Method are used to model SOFCs at the macroscale level. Multiscale modeling is a promising tool for fuel cell research. COMSOL Multiphysics, based on the Finite Element Method, as well as FLUENT, based on the Finite Volume Method, are examples of commercial coded for analysis of coupling different physical models at different scales. Multiscale modeling increases the understanding for detailed transport phenomena, and can be used to make a correct decision on the specific design and control of operating conditions.

A model that describes physical (mass-, heat- and momentum) phenomena inside an anode-supported SOFC is developed, to deeply understand the effect of design and operating parameters. A two-dimensional numerical calculation procedure (CFD approach) is applied in this work. This study focuses on the effect of ionic electronic conductivity, inlet temperature, surplus of oxygen, current density, count flow and internal reforming reactions if hydrocarbon fuels are supplied. The considered cell includes interconnect, air- and fuel channels, anode, cathode and electrolyte. Temperature dependent physical properties are taken into account as well. The temperature distribution in the solid phase and the gas phase are calculated separately, based on the local temperature non-equilibrium (LTNE) approach. The basic model is extended to study the effect of internal reforming reactions.

1.4 Outline of the thesis

The overview of the thesis is presented in chapter 1. Chapter 2 contains a literature survey, where the early fuel cell development, the future potential and different types of fuel cells are presented. Modeling of different transport processes at different scales is presented. The developed mathematical model is introduced in chapter 3, with a breakdown to governing equations, source terms and boundary conditions. The results are presented in chapter 4 and the related conclusions are drawn in chapter 5. The ideas for future work are outlined in chapter 6.

Chapter 2

Literature survey and problem statement

In this chapter a short introduction to fuel cells is given. A description of the early development by C. F. Schönbein and W. R. Grove, as well as the future potential is presented. Basic information about fuel cell technology, with focus on SOFCs is introduced. An introduction will be given to fuel cell modeling at different scales as well as different transport processes. Finally internal reforming reaction kinetics is outlined.

2.1 Introduction to fuel cells

Fuel cells directly convert the free energy of a chemical reactant to electrical energy and heat. This is different from a conventional thermal power plant, where the fuel is oxidized in a combustion process combined with a conversion process (thermal-mechanical-electrical energy), that takes place after the combustion. Fuel cells can have energy conversion efficiencies higher than heat engines, since no Carnot cycle efficiency limitation occurs [1]. If pure hydrogen is used, no pollution of air and environment occurs at all, because the output from the fuel cells is electricity, heat and water. Fuel cells do not store energy as batteries do [2]. A fuel cell consists of two electrodes: one anode for fuel and one cathode for oxidant. The electrodes are separated by the electrolyte and connected into an electrically conducting circuit. A gas or liquid flow, with fuel or oxidant, is transported to the electrode, which should be permeable via a porous structure. Unit cells are organized together into stacks [3].

The fuel cell is not a new invention, because the electrochemical process was discovered already in 1838-39. The interest in fuel cells has been growing exponentially, which is evident from the amount of published scientific papers, after year 2000 [4]. Among various types of fuel cells (FCs), the solid oxide fuel cell (SOFC) has attained significant interest due to its high efficiency and low emissions of pollutants to the environment. High temperature operation offers many advantages, such as high electrochemical reaction rate, flexibility of using various fuels and toleration of impurities [5]. Fuel cell systems are still an immature technology in early phases of development, as can be noted due to lack of a dominant design, few commercial systems and a low market demand. The creation of strategic niche markets and search for early market niches are of a vital importance for the further development. It is expected that mass production will start when a dominant design is found, and then production cost will significantly decrease due to the economy of scale [4].

The ideal amount of energy that can be converted into electrical energy can be described by the Gibbs free energy change of a chemical reaction [3]:

$$\Delta G = -n \cdot F \cdot \Delta V_0 \tag{1}$$

where n is the number of electrons involved in the reaction, F is the Faraday constant and ΔV_0 is the voltage of the cell for thermodynamic equilibrium in the absence of current flow.

2.1.1 Historical development

The principle behind fuel cells dates back to 1838 when the Swiss-German scientist Christian Friedrich Schönbein (professor at Basel University) tried to prove that currents were not a result of two substances coming into "mere contact" with each other, instead the current were caused by a "chemical action", published in "*The London and Edinburgh Philosophical Magazine and Journal of Science*" 1838. In 1839 he published a conclusion based on experiments on platina wire, and how it could become polarized or depolarized depending on the surroundings. Fluids, separated by a membrane, were tested, with different gases dissolved in each compartment. No current was achieved when gold or silver wires were used. It was concluded that "*the chemical combination of oxygen and hydrogen in acidulated (or common) water is brought about by the presence of platina in the same manner as that metal determines the chemical union of gaseous oxygen and hydrogen*" [6].

Not only Schönbein was working on the principle behind fuel cells, Sir William Robert Grove (Royal Institution of Great Britain) performed experiments with a set-up, where two platinum electrodes were halfway submerged into a beaker of aqueous sulphuric acid and tubes were inverted over each of the electrodes, one containing oxygen gas and one hydrogen, published in "*Philosophical Magazine and Journal of Science*" 1839. As the tubes were lowered, the electrolyte was displaced by the gases, leaving only a thin coating of the acid solution on the electrode. A galvanometer indicated a flow of electrons between the two electrodes. The current decreased after some time, but could be restored by renewing the electrolyte layer. Grove concluded in 1842 that the reaction rate was dependent on the "surface of action", i.e., the area of contact between the gas reactant and a layer of liquid electrolyte thin enough to allow the gas to diffuse to the solid electrolyte. Platinum particles deposited on a solid platinum electrode were used to increase the surface area. Grove's goal of electrolyzing water by hydrogen and oxygen was achieved with 26 cells connected in electrical series. Grove was counted according to [6] as the fuel cell inventor. The first fuel cell was called a "gaseous voltaic battery".

SOFC was developed in 1937 by Bauer and Preis, for the need of more manageable electrolyte. Davtayan evolved (in 1946) the Molten Carbonate Fuel Cell (MCFC) with the goal of using coal as fuel and a solid ionic conductor was used as electrolyte and the working temperature was 700 °C. Davtayan is not only the inventor of the MCFC, he also developed a fuel cell with alkaline electrolyte and a low working temperature and atmospheric pressure, i.e., the Alkaline Fuel Cell (AFC), in 1946. It should be mentioned that AFCs were used in the Apollo space program to supply electricity for life support, guidance and communications for the module and water support for the two weeks missions on the moon. Kodesch and Marko evolved the Direct Methanol Fuel Cell (DMFC) in 1951 using carbon electrodes. Fuels such as aldehyde (formaldehyde) and alcohols (methanol and ethanol) could be used. The Polymer Electrolyte Membrane Fuel Cell (PEMFC) was developed to avoid the problem with sealing and circulating a liquid alkaline electrolyte (in AFCs) in 1960 by General Electric. The Phosphoric Acid Fuel Cell (PAFC) was evolved to use reformed natural-gas as fuel in the TARGET program (Team to Advance Research for Gas Energy Transformation), a research program sponsored by mostly American gas companies. This program was initiated in 1967 and a demonstration on a working fuel cell operating on natural-gas took place in 1975 [6]. It can be concluded that the development of new fuel cell types have been by avoiding problems with existing types.

2.1.2 Future fuel cell potential

International Energy Agency (IEA) has concluded in many reports that fuel cells will be a key component in a future sustainable energy system. Fuel cell systems including niche applications or a market where fuel cells bring an added value are already competitive, compared to competing energy systems. About 80 percent of the energy resources traded today are fossil (coal, oil and natural-gas). These resources are limited and the fossil energy sources will sooner or later be depleted, starting with oil. Many of the energy conversion technologies used today are energy inefficient, compared to fuel cells [4].

A new technology is usually introduced into the market in niches where the new and non-traditional characteristic of the technology provides sufficient added value to compensate for the high cost [4]. During recent years, there have been increasing interests to use fuel cells as auxiliary power units (APUs) in on-board applications, for example in luxury passenger vehicles, police vehicles, contractor trucks, specialized utility trucks, recreational vehicles, refrigeration vehicles, and heavy trucks, military vehicles, tourist- and leisure boats. In a short term, on-board hydrogen production makes it possible to have a more efficient use of energy and current fuel refilling system. Gasoline, kerosene or diesel can still be used as fuel and only one fuel refilling system is then needed on-board the vehicle. The vehicle industry is known to be conservative regarding fuels and usage of diesel as fuel will promote the fuel cell commercialization [7]. The fuel can be reformed from any hydrocarbon to pure hydrogen. FC APUs can be seen as a good transition state to reach the aim of hydrogen economy in mobile applications. The PEMFC APUs can be designed from a few hundred Watts for yachts, up to more than 10 kW for the heavy trucks [7-8]. Calculated estimated target cost, for different fuel cell niche markets, can be seen in Table 1:

Table 1: Willingness To Pay (WTP) for different FC niche markets [4].

Niche Market	WTP (EUR/kW)	Main added value
<i>Space applications</i>	~30 000	High gravimetric density
<i>Military applications</i>	3000-7000	Low noise
<i>APUs</i>	1000-2000	Low stand-by losses
<i>Portable applications</i>	500-2000	Grid independence and high volumetric energy density
<i>Combined heat and power</i>	500-1200	High efficiency and low emissions
<i>Buses</i>	200-300	Zero local emissions and resource flexibility
<i>Cars</i>	50-150	Zero local emissions and resource flexibility

IEA made predictions and prognoses for the future fuel cell potential. The future potential in the stationary sector can be seen in Fig. 1. It should be mentioned that scenario A considers weak carbon dioxide policies, liberalized markets, and market-driven technology development. Scenario B counts on strong carbon dioxide policies in Kyoto countries and rapid technology development, scenario C is like B, but with weaker technology development. Finally scenario D includes world wide strong carbon dioxide policies and a rapid technology development [9].

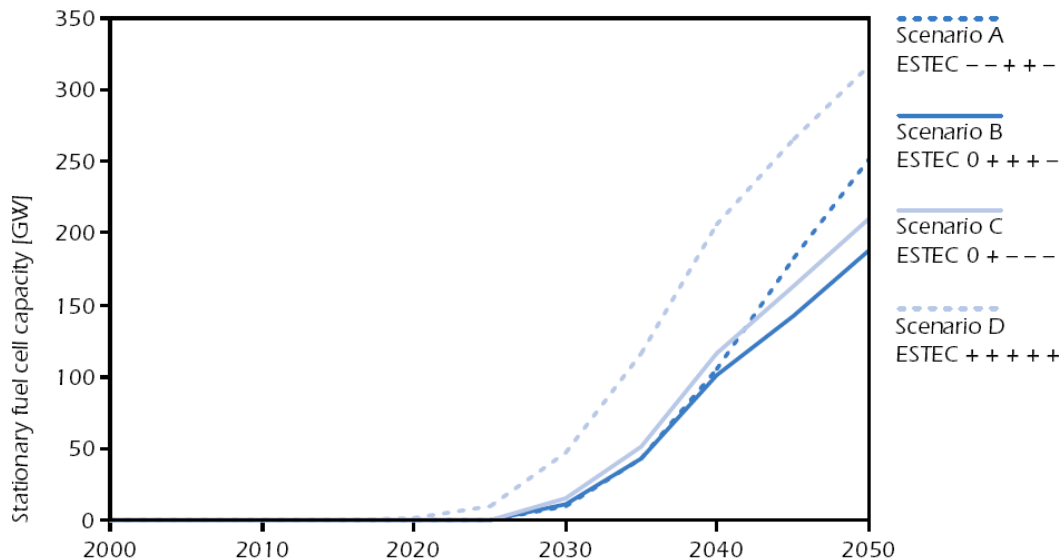


Figure 1: Global stationary fuel cell use in the IEA ESTEC scenarios [9].

2.2 Various types of fuel cells

Different fuel cell types and their characteristics are summarized in Table 2.

Table 2: Fuel Cell types and their characteristic [3, 4]

	AFC	PAFC	PEMFC	SOFC	MCFC
<i>Electrolyte:</i>	Alkaline – potassium hydroxide	Phosphoric acid	Polymer membrane	Ceramic membrane	Molten carbonate
<i>Mobile ion:</i>	OH ⁻	H ⁺	H ⁺	O ²⁻	CO ₃ ²⁻
<i>Producing water at:</i>	Anode	Cathode	Cathode	Anode	Anode
<i>Operating temperature:</i>	50-200 °C	~220 °C	70-100 °C	500-1000 °C	~650 °C
<i>Current densities [A/cm²]:</i>	0.1-0.4	0.15-0.4	0.4-0.9	0.3-1.0	0.1-0.2
<i>Voltage interval [V]:</i>	0.85-0.6	0.8-0.6	0.75-0.6	0.95-0.6	0.95-0.75
<i>Stack Efficiency (LHV) [%]:</i>	45-60	45-65	40-70	45-75	50-65
<i>Typical Applications & Power Output:</i>	Spacecraft 1-15 kW Niche vehicles 20 kW	Stationary 200 kW	Vehicles 100 kW Stationary 1-10 kW Portables < 1.5 kW	Stationary 5-200 kW APUs ~5 kW	Large stationary 200 kW-MW
<i>Fuel:</i>	Hydrogen	Hydrogen	Hydrogen	Methane Hydrogen	Methane Hydrogen
<i>Interconnect:</i>	Metal	Graphite	Carbon or Metal	Stainless steel or Nickel	Nickel ceramic or Steel
<i>Electrodes:</i>	Transition metals	Carbon	Carbon	Perovskite and Perovskite/ metal cerment	Nickel and Nickel oxide
<i>Catalyst:</i>	Platinum	Platinum	Platinum	Nickel (Electrode material)	Nickel (Electrode material)
<i>Product Heat Management:</i>	Process Gas +Electrolyte Circulation	Process Gas +Liquid cooling medium or steam generation	Process Gas + Liquid Cooling Medium	Internal Reforming + Process Gas	Internal Reforming + Process Gas
<i>H₂:</i>	Fuel	Fuel	Fuel	Fuel	Fuel
<i>CO:</i>	Poison	Poison	Poison	Fuel	Fuel
<i>CH₄:</i>	Poison	Dilutent	Dilutent	Fuel (after reforming)	Dilutent
<i>CO₂ & H₂O:</i>	Poison	Dilutent	Dilutent	Dilutent	Dilutent
<i>S (H₂S & COS):</i>	Poison	Poison	?	Poison	Poison

2.3 Solid Oxide Fuel Cells (SOFCs)

SOFCs can work with a variety of fuels, e.g., hydrogen, carbon monoxide, methane and combinations of these [10]. Oxygen is reduced in the cathode, eqn. (2). The oxygen ions are transported through the electrolyte, but the electrons are prevented to pass through the electrolyte. The electrochemical reactions, eqns. (3)-(4), take place in the anodic TPB. Methane needs to be reformed, eqn. (5), before the electrochemical reactions [11]. Carbon monoxide can be oxidized in the electrochemical reaction, eqn. (4), but can also react with water eqn. (6). The reactions described here are the overall reactions, more detailed reaction mechanisms can be found in [11-15]. Note that methane is not participating in the electrochemical reactions at the anodic TPB, it is catalytically converted, within the anode, into carbon monoxide and hydrogen, which are used as fuel in the electrochemical reactions [12]. Hybrid concept involving a combination of a gas turbine and a fuel cell can be developed with high conversion efficiency [3].



SOFCs have in general either planar or tubular configurations. **Planar SOFC** configurations consist of alternating flat plates of a trilayer anode-electrolyte-cathode and interconnect, as seen in Fig. 2. They are normally more compact than tubular ones, i.e., a higher power density per unit volume can be achieved [16]. Planar SOFCs are simpler to fabricate and easier to be constructed into various shapes compared to other type designs. However, there are some problems that need to be solved for this design; the internal stress in cell components arising from heat cycles or thermal shocks and non-homogeneous distribution of temperature inside the cell adding a large internal stress [17]. Planar design needs sealing material to seal the edges of the cell and avoid fuel leakage and air mixing. The glass ceramics and glass are suitable, because they are compatible with the other components at the SOFC working temperature [18].

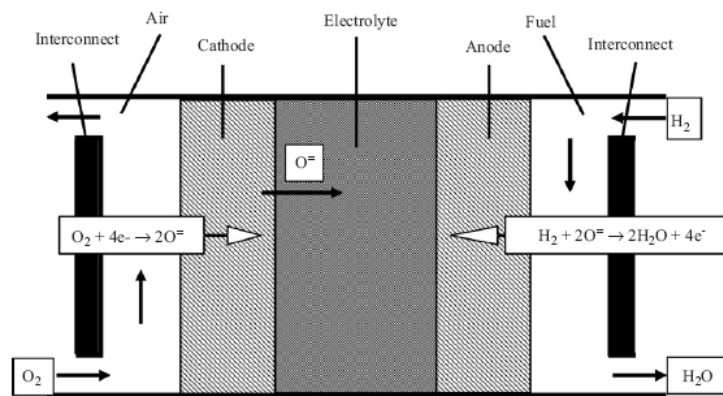


Figure 2: Planar SOFC structure [16].

A **Tubular SOFC** is composed of two electrodes that are sandwiching an electrolyte layer, as seen in Fig. 3. For conventional tubular fuel cells the air flows on the inside of the tube and the fuel on the outside. Tubular fuel cells can be stacked either electrically in series or in parallel [19].

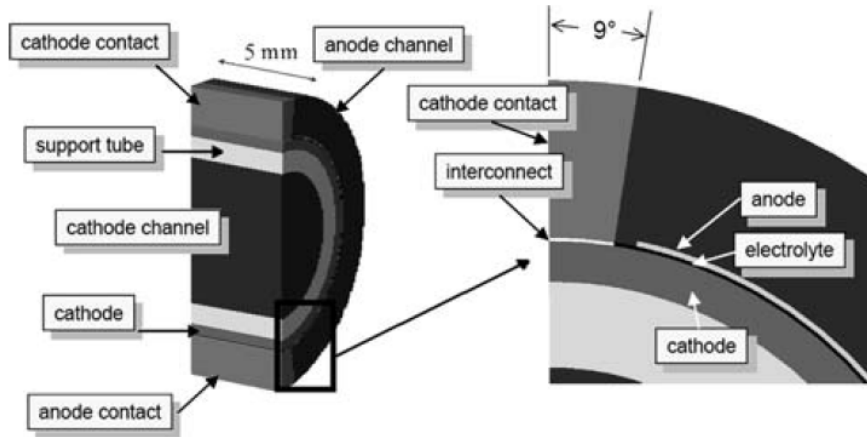


Figure 3: Tubular SOFC structure [20].

Tubular and Planar SOFCs can be either electrolyte-, anode-, cathode- or metal- supported. An electrolyte-supported SOFC have thin anode and cathode ($\sim 50 \mu\text{m}$), and the thickness of the electrolyte is more than $100 \mu\text{m}$. An electrolyte-supported SOFC works preferably at temperatures around $1000 \text{ }^\circ\text{C}$. In an electrode-supported SOFC either the anode (anode-supported) or the cathode (cathode-supported) is thick enough to serve as the supporting substrate for cell fabrication, normally between 0.3 and 1.5 mm . The electrolyte is in this configuration thin (could be as thin as $10 \mu\text{m}$ [21]). In a monolithic configuration a layer of anode and cathode material is corrugated on either side of the trilayers to form fuel- and air-channels [16].

The SOFC research in the last years has been focused on lowering the operating temperature. Positive aspects of development in this direction are that the start-up and slow-down time decreases, design and materials requirement are simplified, corrosion rates are significantly reduced and the stack lifetime are prolonged. Metallic material, for example stainless steel (=low cost), can be used for interconnects and construction materials. This reduces the construction cost and increase the stability of the fuel cell [22-23]. Lowering the operating temperature to an intermediate range will cause an increase of both ohmic- and polarization losses in the electrodes. This requires development of a highly active electrolyte that has a low polarization loss at intermediate temperatures [24]. Possible electrolyte materials could be doped ceria or doped lanthanum gallate [22].

Electrode-supported design makes it possible to have a very thin electrolyte, i.e., the ohmic losses decreases and the temperature can be lowered to $600\text{-}800 \text{ }^\circ\text{C}$. Fuel cells working at that temperatures are classified as intermediate temperature (IT) ones [1, 2] if compared to conventional SOFCs that operate at $800\text{-}1000 \text{ }^\circ\text{C}$ [6]. The electrolyte contains yttria-stabilized zirconia (YSZ), the cathode strontium doped lanthanum manganite (LSM) and the anode nickel/YSZ [1].

Low temperature (LT)-SOFCs in the range of $300\text{-}600 \text{ }^\circ\text{C}$ is under development, the challenge is to increase the ionic conductivity in the electrolyte. Low temperatures make it possible to use cheaper materials throughout the fuel cell system. An approach with material development on the nanoscale is expected to be very promising [7].

2.4 SOFC modeling development

Before designing and constructing a model, it is important to specify what one wants to know, how accurate and why. The choice of computational methods must come from a clear understanding of both the information being computed and the chemical system. It is also needed to be aware of what approximations being made and which ones being significant [25].

2.4.1 Micro-, meso- and macroscale approaches

An SOFC can be described by different length scales: system scale ($\sim 10^2$ m), component scale ($\sim 10^1$ m), material aspect at the fuel cell/constituent ($\sim 10^{-2}$ m), flow/diffusion morphologies ($\sim 10^{-3}$ m), material structure/interface ($\sim 10^{-6}$ m), and functional material levels ($\sim 10^{-9}$ m). Not only proper length scales are needed to describe various parts of an SOFC, also different time scales need to be considered. Cell charging and cathode gas thermal diffusion are in 10^{-3} s, convective transport is in 10^{-1} s, cell heating and anode streamwise thermal diffusion are in 10^3 s and cathode streamwise thermal diffusion is in 10^4 s [5]. A relation between time- and length scales with proper modeling methods can be seen in Fig. 4.

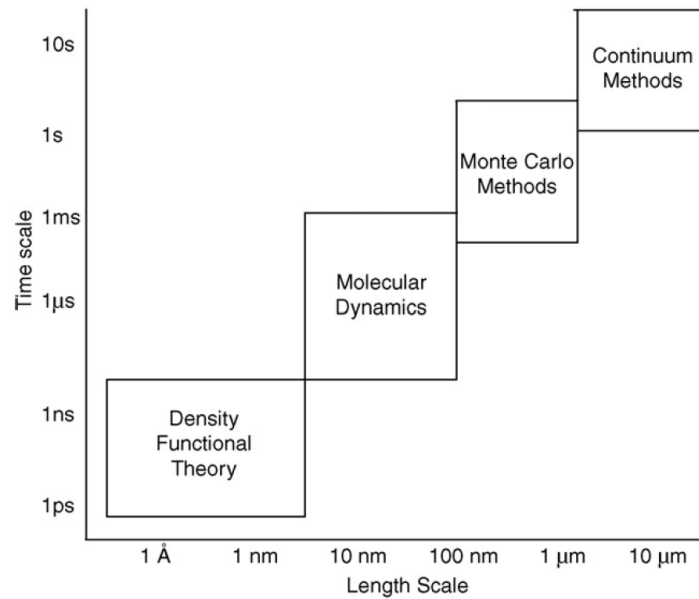


Figure 4: Characteristic time and length scales for various methods [26].

Research of the physical phenomena is based on different levels of scales: micro-, meso- and macroscales. The microscale model corresponds in many cases to the atom or molecular level as thermo- or fluid dynamics and detailed chemical reactions are studied. The microscale does not need to be as small as the size of the molecules. A mesoscale model corresponds to a larger scale than a particle but a smaller one than the facility or the global flow field. Macroscale models match to the global flow field. Microscale modeling is in general more related to theoretical knowledge compared to macroscale modeling that is more related to empirical data. Empirical parameters for macroscale models could be based on the results from micro- or mesoscale models [12].

Instantaneous flow around individual moving particles can be calculated in microscale models. Flows corresponding to calculation cells, larger than particles but smaller than global flow field, are calculated with mesoscale models. Trajectories of individual particles are calculated with particle motion equations for microscale modeling. The flow field is in mesoscale modeling divided into a number of small cells, but not as small as the particle size [12].

Different methods have been developed to describe different scales. Methods that have been used for SOFC modeling are listed in Table 3, based on micro-, meso- and macroscales.

Table 3: Computational methods arranged after scales [12, 26-40].

Microscale	Mesoscale	Macroscale
Density Functional Theory (DFT)	Kinetic Monte Carlo (KMC)	Finite Element Method (FEM)
Quantum Chemistry (QC)		Finite Volume Method (FVM)
Lattice Boltzmann Method (LBM)	Brownian Dynamics (BD)	Finite Difference Method (FDM)
Molecular Dynamics (MD)		Spectral Methods (SM)
Mechanistic Models (MM)	Dissipative Particle Dynamics (DPD)	
Dusty Gas model (DGM)		
Ficks model (FM)		
Stefan-Maxwell model (SMM)		

2.4.2 SOFC modeling at microscale

Frayret *et al* [27] simulated microscopic aspects of oxygen diffusion in the ceria-based material in the ionic conductor with the Density Functional Theory (DFT). This methodology is a good tool to study the connection between dopant ionic radius and diffusion at the atomistic scale. DFT is an “ab initio” method where the material properties are described by solutions of the Schrödinger equations. DFT models have a characteristic length scale of Å – nm and a time scale of ps – ns.

Cheng *et al* [28] simulated the oxygen ion-hopping phenomenon inside a YSZ electrolyte with Molecular Dynamics (MD). MD can be used to model grain boundary structure, specific heat capacity and molecular structure. Systems up to 10^5 atoms and a time scale of the order of ten ns can be modeled [29].

The Lattice Boltzmann Method (LBM) is used to model mass transport of gases inside the porous anode of an SOFC. The porous structure is based on SEM (scanning electron microscope) images, which are converted to digital form. Advantages of the LBM model are that a detailed analysis of mass transfer can be carried out for the actual anode microstructure; this means that tortuosity is not used as a fitting parameter. LBM approach is according to an investigation in [30] accurate enough to model concentration polarization in 2D. By changing the number of void spaces present in the solid matrix the porosity in the LBM is varied.

Dusty Gas model (DGM), Ficks model (FM) and Stefan-Maxwell model (SMM) are developed in [31], in order to predict the concentration over potential inside an SOFC anode. DGM and FM consider molecular diffusion, Knudsen diffusion and the effect of a finite pressure gradient. The flux ratio in DGM depends on the square-root of the gas molecular weight, but it does not for FM. Explicit analytical expressions describing fluxes can be used in FM. The SMM can be seen as a simpler model since it does not consider the Knudsen diffusion. DGM is the most appropriate model for H₂-H₂O and CO-CO₂ system. However, it is only required to use it when the operating current density is high. Ni *et al* [12, 32] studied the effect of micro-structural grading on SOFC performance with a DGM to analyze the coupled phenomena of mass transfer and electrochemical reactions in the SOFC electrodes.

There is a big difference between DFT/LBM and DGM/FM/SMM. For the last ones empirical modifications (for example porosity and tortuosity) are used to fit the model to experimental data, while in DFT/LBM one uses theoretical expressions for the calculations [33, 34].

2.4.3 SOFC modeling at mesoscale

Modak and Lusk [29] applied Kinetic Monte Carlo (KMC) to simulate the open-circuit voltage and electrical double layers of a doped electrolyte. Discrete time increments of varying size are

used to capture diffusion or adsorption in a single step. The physical property data generated by QC and MD can be utilized in the KMC model. Monte Carlo methods have a characteristic length scale of 100 nm – μm and a time scale of ms – s [35].

Huang *et al* [36] employed COMSOL Multiphysics (FEM) to model the multiphysics processes in the SOFC cathode-electrolyte interface considering the geometry and detailed distribution of the pores and the ionic conducting phase. The charge transfer rate, electrical conduction and ion conduction are governed on a modeling domain abstracted from actual materials encountered in the application.

2.4.4 SOFC modeling at macroscale

Cheng *et al* [28] used the Finite Element Methods (FEM) and the commercial software COMSOL Multiphysics to solve the flow equations for macroscopic transport phenomena. Navier-Stokes equations are used to describe the flow conditions in the air and fuel channels and Darcy law describes the flow conditions in the porous layer. FEM has a characteristic time scale of 1 s and above [27].

A clear relationship between underlying physical conditions and numerical algorithm has made the Finite Volume Method (FVM) a popular method for commercial codes such as PHOENICS, FLUENT, CFX and STAR-CD [37]. Pasaogullari and Wang [38] as well as Autossier *et al* [39] used FLUENT to solve the equations of momentum, mass, energy, multicomponent species and electrochemical kinetics for an SOFC. Hussain *et al* [40] employed the FVM to model the transport of multi-component species inside porous SOFC anodes.

2.4.5 SOFC modeling integration issues

Multiphysics modeling considers interaction and coupling between two or more physical disciplines. Physical problems can often be described with a set of partial differential equations. The coupled partial differential equations can be solved simultaneously in physical domains for corresponding physical phenomena. Fuel cell operation depends on complex interaction between multi-physics such as multi-phase fluid flow, mass transport, heat transfer and electrochemical reactions [41]. Two basic integration approaches can be found: hierarchical method and hybrid and cocurrent method. The hierarchical modeling starts at higher resolution (smaller scale) and properties are extracted and used as input to the next level method. The hierarchical methods are today the most developed methods for multiscale modeling [27]. Three different methods are used for hybrid approaches to describe various regions of the material with the appropriate time and length scale resolutions. The hybrid methods that permit cocurrent simulations are promising for the future development, since only one calculation needs to be performed, however, it requires more computational power compared to the hierarchical methods [27].

The particle size in SOFCs is in the sub-micron scale, and the TPBs are in nanoscale. The morphology and properties of these scales are important for the performance of the fuel cell, since they control how much of the Gibbs free energy being available for use. It means that the science at nanoscale is critical to the performance at a system-scale. A robust design and multi-scale analysis consider those nano-details as well as macro system level [42].

Tseronis *et al* [43] developed a multiscale concept, where the microscale DGM is used to describe mass transfer in porous media and FEM based COMSOL Multiphysics is used for the numerical solution of the governing equations. DGM is used for porous media transport, Butler-Volmer equation for electrochemistry, a multi-step model for heterogeneous chemistry and FLUENT is used to couple the different physical descriptions together [14].

Cheng *et al* [28] and Pasaogullari and Wang [38] introduced multiscale-concepts; however, they did not mention how the different scales interact with each other. It is frequently stated in the literature that data or property constants can be obtained from smaller scale and then used in a

model made in a larger scale. However, information about the construction of this coupling is rare [12,14, 26-27].

2.5 Transport processes

SOFCs can be examined from different points of view; as an electrochemical generator in a viewpoint of electrochemical modeling at continuum level, as a heat and mass exchanger in a viewpoint of fluid dynamics and transport phenomena, as a chemical reactor in viewpoints of chemical reactions depending on fuel composition and heat effects associated with the electrochemical conversion [16].

The number of fuel gases transported to the active surface for the electrochemical reactions are governed by different parameters, such as porous microstructure, gas consumption, pressure gradient between the fuel flow duct and the porous anode and the inlet conditions [35]. The gas molecules diffuse to the TPB, where the electrochemical reactions take place. The supply of reactant can be the rate limiting step, since the gas molecule diffusion coefficient is much smaller than for ions. The charge transfer chemistry at the interface between the electrolyte and the anode proceeds on the basis of the hydrogen concentration. The hydrogen concentration depends on the transport within the porous anode and the heterogeneous reforming reaction chemistry. The concentration of the fuel gases, CH₄, CO and H₂, decreases along the length of the fuel channel while the concentration increases for H₂O and CO₂. As a result the current density decreases along the fuel channel [10].

2.5.1 Mass transport

Transport in the porous electrodes occurs in the gas phase, integrated with the chemical reforming reactions at the solid active surface. The electrodes are porous and mass transfer is dominated by gas diffusion [44]. The electrolyte has two functions: to transport oxide ions from the electrolyte to the anode and to block electron flow from the anode to the cathode [11]. The flow of electronic charge through external circuit balances the flow of ionic charge through the electrolyte and electrical power is produced [45]. The interconnect can be assumed to be impermeable for gases. Electron transport needs to be considered since the current from the SOFC is collected [16].

Ficks law is the simplest diffusion model, and used for dilute or binary systems [46]. In the literature the Stefan-Maxwell model is commonly used to calculate the diffusion in a multi component system. In some references the Stefan-Maxwell model is combined with the Knudsen diffusion term (frequently called the Dusty Gas model or extended Stefan Maxwell equation) [14,47-51], to predict the collision effects between the gas molecules and the solid porous material. In other models this effect is neglected [52].

To account for the increased diffusion length due to the tortuous paths of real pores in the porous materials, different approaches can be found in the literature [53]:

$$D_{i,eff} = \varepsilon^t \cdot D_i \quad (7)$$

$$D_{i,eff} = \frac{\varepsilon}{t} \cdot D_i \quad (8)$$

where D_i is the ordinary diffusion coefficient, $D_{i,eff}$ the diffusion coefficient in the porous medium, ε the porosity and t the tortuosity. Similar expressions can be found for the Maxwell Stefan Diffusion coefficient in porous material [48, 50].

Knudsen diffusion

For the porous layer, molecular diffusion is predominant for the case with large pores, whose size is much bigger than the free path of the diffusion gas molecules [51], i.e., the Stefan-Maxwell

model describes the transport processes with a good enough accuracy. The Knudsen diffusion is used when the pores are small in comparison to the mean free path of the gas. For Knudsen diffusion, molecules collide more often with the pore walls than with other molecules. The Knudsen diffusion coefficient can be calculated using a kinetic theory that relates to the diameter of the pore and the mean free part of the gas according to [50]:

$$D_k = \frac{u \cdot r'}{6} \quad (9)$$

where D_k is the Knudsen diffusion coefficient, r' is the average pore radius and u is the velocity of the gas molecules. If the pores are straight and round, the diffusion coefficient of component i is [50]:

$$D_{ik} = 97.0 \cdot r' \cdot \sqrt{\frac{T}{M_i}} \quad (10)$$

where D_{ik} is the Knudsen diffusion coefficient for molecule i , T the temperature and M_i the molecular weight. To calculate the mean pore radius (r'), the surface area of the porous solid and the porosity is used [50]:

$$r' = \frac{2 \cdot \varepsilon}{SA \cdot \rho_B} \quad (11)$$

where SA is the surface area of the porous solid and ρ_B is the bulk density of the solid particle. It is possible to account for the tortuous path of the molecule, by calculating the effective Knudsen diffusion coefficient [50]:

$$D_{ik(eff)} = D_{ik} \cdot \left(\frac{\varepsilon}{t}\right) \quad (12)$$

where $D_{ik(eff)}$ is the effective Knudsen diffusion coefficient. Ordinary diffusion and Knudsen diffusion may appear on the same time and can be calculated as [46,50]:

$$\frac{1}{D_{i(eff)}} = \frac{1}{D_{ij(eff)}} + \frac{1}{D_{ik(eff)}} \quad (13)$$

2.5.2 Momentum transport

The governing equation for momentum transport is the Navier-Stokes equation in the fuel channels and the Darcy equation for the porous electrodes [35, 51]. Connection between Navier-Stokes and Darcy equation with the Darcy-Brinkman approach is described in chapter 3.2.1.

The physics of laminar and turbulent incompressible flow are well described by the Navier-Stokes equation, and it is common practice to assume laminar flow for fuel cell gas channels due to the low velocities, which decreases the computational cost significantly [53].

Darcy equation describes the balance between the force from the pressure gradient and the frictional resistance from the solid material. It should be noted that the Darcy equation expresses the flow in the porous structure well away from the walls. No-slip conditions at neither the walls nor the resulting boundaries are well described by the Darcy equation, however the Darcy equation can be modified with the so-called ‘‘Brinkman term’’ to enable modeling of the boundary/interface conditions as well. This is further described in [49, 54].

2.5.3 Heat transport

The heat transfer inside SOFCs includes various aspects such as convective heat transfer between the solid surfaces and the gas stream, conductive heat transfer in solid and porous structures. Heat generation occurs due to the electrochemical reactions at the active surfaces in the interface between the electrolyte and electrodes [55], and due to the internal reforming reactions of methane in the porous anode and of carbon monoxide in the porous anode and in the fuel channel [56]. Accurate temperature prediction within SOFCs is essential for predicting and optimizing the overall cell performance as well as avoiding thermo-mechanical degradation [57].

A very common assumption in SOFC modeling is to assume local thermal equilibrium (LTE) [46, 51, 57], however, some typical conditions found in the porous SOFC electrodes bring this assumption into question: (1) very low Reynolds number flow, (2) presence of volumetric heat generation and (3) large difference in thermal conductivity between the gas- and solid phase. A local temperature non-equilibrium (LTNE) approach is developed in [57] to predict and model the temperature difference between the solid- and gas phases within the porous electrodes.

Most of the heat within SOFCs is generated near the electrode/electrolyte interface and it is dissipated by: (1) conduction in the solid matrix, (2) heat transfer from the solid to the gas phase by convection within the pores and (3) advection of the gas through the micro-pores to the flow channel [57]. The LTNE approach is included in the study and more information can be found in chapters 3.2.3 and 3.3.3.

Effective transport parameters for the porous material need to be calculated when a LTE approach is used, the thermal conductivity (k_{eff}) and specific heat ($c_{p,eff}$) can be specified as [51]:

$$k_{eff} = \varepsilon \cdot k_f + (1 - \varepsilon) \cdot k_s \quad (14)$$

$$c_{p,eff} = \varepsilon \cdot c_{p,f} + (1 - \varepsilon) \cdot c_{p,s} \quad (15)$$

where ε is the porosity, eff means effective, s means solid and f means fluid (gas) phase.

2.5.4 Integration issues

The mass-, heat-, momentum transport and the reaction rate are dependent on each other. The fluid properties and the momentum transport (flow field) depend on the temperature and concentrations. The (electro-) chemical reaction rate depends on temperature, concentrations and available surface area for catalyst reaction. The chemical reactions generate and consume heat, i.e., the temperature distribution depends on the chemical reaction rate, as well as on the solid and the gas properties (for example the heat capacity and the conductivity) [1].

2.6 Electrochemical reactions

Electrochemical reactions occur mainly at the TPBs, i.e., the region where the electrode and electrolyte meet. Ions migrate in the ionic phase, conduction of electrons occurs in the electronic phase and transport of gas molecules takes place in the porous part of the electrodes. A larger TPB area gives more reaction sites (= lower activation polarization in the electrodes). With a small electrode thickness the TBP area becomes even more important [52].

The total pressure is lower close to the cathode/electrolyte interface, compared to other parts of the cathode due to the consumption of oxygen molecules at TPBs. This gradient makes the transport of oxygen from the channel towards the electrolyte easier. The TPB area in the electrode depends on the particle diameter. A reduction of the particle diameter increases the TBP area, at the same time the Knudsen diffusivity and the flow permeability are reduced. In [52] it is found that most of the electrochemical reaction occurs within 10 μm for the anode and 50 μm for the cathode when the mean particle diameter is 1 μm [52].

The reaction rate (in mol/(m²s)) at the electrochemical active area is given as [14, 53, 58]:

$$r_{H_2} = \frac{-i}{2 \cdot F} \quad (16)$$

$$r_{H_2O} = \frac{i}{2 \cdot F} \quad (17)$$

$$r_{O_2} = \frac{-i}{4 \cdot F} \quad (18)$$

where i is the current density and F the Faraday constant.

2.7 Internal reforming reactions

Internal reforming reactions inside SOFC porous anodes enable the conversion of methane into hydrogen and carbon monoxide. The heat, needed by the internal reforming reactions, is generated in the electrochemical reactions at the active surface (TPB) between the porous anode/electrolyte and cathode/electrolyte. A good heat transfer (in terms of short heat transfer distance between heat generation and consumption within the fuel cell) can be achieved, the conversion efficiency is increased. Hydrogen and carbon monoxide can be oxidized as soon as they are produced by the reforming reactions and steam that is produced by the electrochemical reaction (eq. (3)) can be used in the reforming reactions [35, 59].

The reforming of hydrocarbon fuels could either take place before the fuel cell stack, in an external pre-reformer or inside the cell in the anode (internal reforming). A pre-reformer needs extra added steam, since it can not use the steam generated in the electrochemical reactions, and the steam reforming reaction takes place over ceramic-supported nickel catalysts. The internal reforming reactions decrease the requirement for cell cooling (less surplus of air) and less steam for the reforming reactions is needed and finally it offers advantages with respect to the capital cost. Up to half of the heat produced by the oxidation reaction (exothermic) could be “consumed” by the reforming process. This would improve the system electrical efficiency [56].

In a conventional SOFC (with nickel content of about 50 vol.% and operating temperature of 800-1000 °C) the endothermic reaction is very fast. This can result in a temperature drop at the inlet of the stack. The temperature gradient results in thermal tensions, which in the worst case causes mechanical failure of the cells [56]. The problem of the tensions and big temperature gradients close to the inlet could be solved with different approaches:

- Lowering the operating temperature to an intermediate range to reduce the steam-reforming reaction rates [60].
- Recycling a part of the anode gas to obtain a dilution of the fuel. The rate of reforming reactions decreases, due to decrease in fuel concentration. A 50 percent recycling results in enough steam for reforming reactions and the cost for a separate water supply is saved [56].
- The anode material can be designed with the aim of a decreased steam reforming activity. Until now these new SOFC materials (such as iron or copper) have too low electronic conductivity to meet the real world requirements. When nickel is replaced during the fabrication process with for example iron, a less catalytic active anode regarding the reforming activity, is constructed. This is in the short term a promising method, and this approach is based on well-established production processes. Other researches replace nickel with copper and the same effect has been reached [56].

The reforming reactions occur in the porous anode. The reaction rates can be described with simplified global expressions as well as detailed expressions for surface chemical reactions, and this will be described in the following subchapters.

2.7.1 Surface chemistry

An SOFC anode is normally fabricated as a porous metal-ceramic composite, where the gas, ceramic and metal phases occupy roughly 30 percent of the volume each, the characteristic pore dimensions are in the order of $1\ \mu\text{m}$ [15]. Significant disparities are seen in the rate constants, rate expressions, and activation energies between different numerical studies on the catalytic reforming activity on Ni-YSZ in literature [61]. Knowledge of the catalytic mechanism considering oxidation of hydrocarbons is counted as a key importance for designing a anode material with a high efficiency [62].

It is found that the catalytic sites for conversion of methane and the sites for the electrochemical reactions are not the same. The electrochemical reaction occurs at the interface between the anode and electrolyte, and is linked to the reactions where the fuel is activated by chemisorption on the anode nickel surface [63].

The probability for carbon depositions depends on the steam/methane ratio. It has been well established that the key reactions occur over a surface layer of nickel atoms. If a layer of carbon is allowed to build up attached to a nickel crystallite rapid catalyst breakdown can occur, due to the graphite formation. It should be noted that hydrocarbons with a longer coal chain than methane have a higher propensity for carbon deposition. To avoid carbon deposition inside the SOFC anode pre-reforming can be carried out before the fuel enters into the cell at a lower temperature at which carbon deposition does not occur [64].

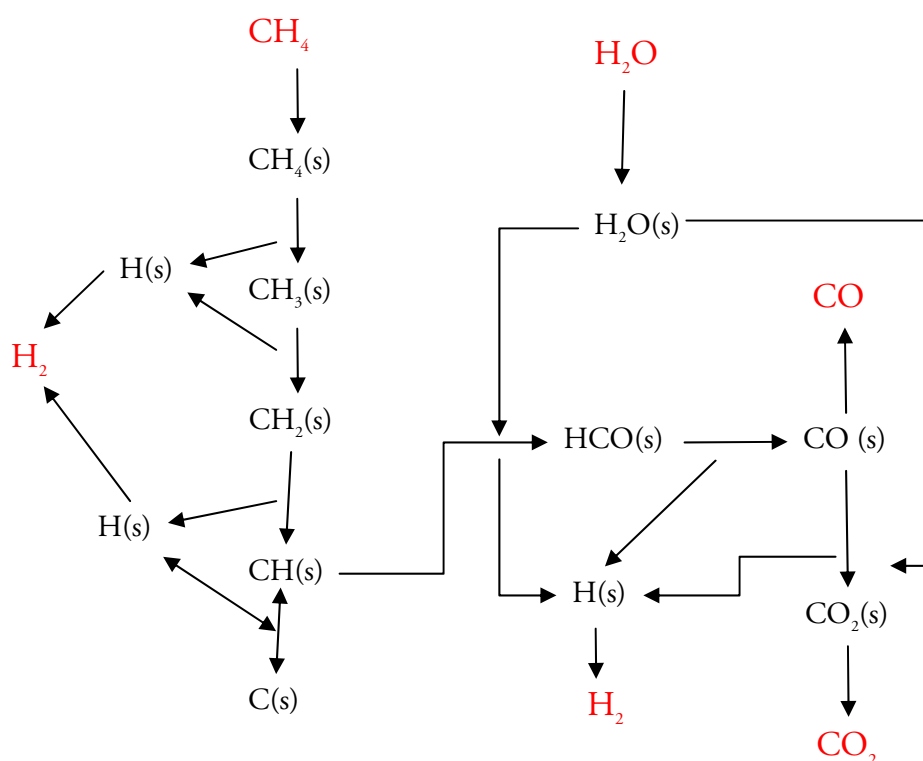


Figure 5: Sketch of a heterogeneous reaction mechanism for methane reforming on Ni-based catalysts. Note that not all the reaction paths from the mechanism in [14] are described in this figure. (s) means that the molecule is in solid phase, i.e., bound to the nickel catalyst which is involved in all the above reactions. All the above reactions in equilibrium are proceeding in two directions. Only the “main” directions are shown to simplify the sketch.

Janardhanan and Deutschmann [14] have developed a multi-step heterogeneous reaction mechanism for Ni catalysts. The mechanism consists of 42 reactions, 6 gas-phase species and 12 surface adsorbed species. The mechanism is elementary in nature and covers the global aspects of reforming, water-gas shift and Boudouard reaction. Most of the expressions are expressed in Arrhenius rate form and are dependent on the surface coverage. The mechanism from [14] is also used in [15, 65]. A sketch of a simplified heterogeneous reaction mechanism can be seen in Fig. 5.

2.7.2 Global kinetics

Methane can be converted to hydrogen and carbon monoxide inside the porous anode with catalytic steam reforming, eq. (5). Carbon monoxide reacts further (inside the anode as well in the fuel channel) with steam to hydrogen and carbon dioxide according to the water-gas shift reaction, eq. (6) [20, 72]. The overall reactions can be written as:



The water-gas shift reaction should be considered to be at equilibrium in the fuel channel. The reaction velocity can be expressed with an equilibrium-limited shift reaction rate expression, first order in carbon monoxide and with arbitrarily high pre-exponential factor as [66]:

$$r_s = k_s \cdot p_{CO} \cdot \left(1 - \frac{p_{CO_2} \cdot p_{H_2}}{K_{e,s} \cdot p_{CO} \cdot p_{H_2O}} \right) \quad (19)$$

where r_s is the reaction velocity of the water-gas shift reaction, k_s the pre-exponential factor, p_i partial pressure for the respectively species and $K_{e,s} = \exp(4276/T - 3.961)$ [66]. Hydrogen reacts with oxygen ions at the anodic TPB and generates steam. As hydrogen is consumed and steam generated the equilibrium water-gas shift reaction proceeds towards the right, i.e., more hydrogen is produced.

The catalytic steam reforming reactions occurs at the surface of the porous structure inside the anode. There is a big variety of reaction rate expressions developed in the literature, which are based on YSZ/nickel cermet anodes with different structure and composition [72]. Four different kinetic expressions and one equilibrium approach with different reaction orders of water are outlined in [67] as:

$$r_{r,Ach} = 4274 \cdot p_{CH_4} \cdot \exp\left(\frac{-82000}{R \cdot T_s \cdot K_e}\right) \quad (20)$$

$$r_{r,Ahf} = 8542 \cdot p_{CH_4}^{0.85} \cdot p_{H_2O}^{-0.35} \cdot \exp\left(\frac{-95000}{R \cdot T_s \cdot K_e}\right) \quad (21)$$

$$r_{r,Lei} = 30.8 \cdot 10^{10} \cdot p_{CH_4} \cdot p_{H_2O} \cdot \exp\left(\frac{-205000}{R \cdot T_s \cdot K_e}\right) \quad (22)$$

$$r_{r,Dre} = \frac{288.52 \cdot p_{CH_4} \cdot p_{H_2O} \cdot \exp\left(\frac{-11000}{R \cdot T_s \cdot K_e}\right)}{1 + 16.0 \cdot p_{CH_4} + 0.143 \cdot p_{H_2O} \cdot \exp\left(\frac{39000}{R \cdot T_s \cdot K_e}\right)} \quad (23)$$

$$r_{r,eq} = 10000 \cdot p_{CH_4} \cdot p_{H_2O} \cdot \left(1 - \frac{p_{CO} \cdot p_{H_2}^3}{K_{e,STR} \cdot p_{CH_4} \cdot p_{H_2O}}\right) \quad (24)$$

where r_r is the reaction rate of steam reforming reaction (in mol/s/m), p is the partial pressure (in bar), R is the ideal gas constant, T is the temperature and K_e the equilibrium constant. The reaction rate is converted to per surface area (mol/s/m²) after multiplying the reaction rate (mol/s/m) with the surface area (SA). Equation (24) describes an equilibrium approach and the reaction orders of the reaction are the same as the molar proportions for the respectively gas species in the global chemical reaction (1 for both methane and water for the forward reaction and 3 for hydrogen and 1 for carbon monoxide for the backward reaction). The reaction order of methane varies between 0.85 and 1. The highest difference in reaction orders is found in the reaction order of water, both negative and positive values exist, however, it has been shown that all these findings could be correct for the chosen operating conditions of the experiment. Small steam-to-carbon (SC) ratio gives positive reaction order of water. SC in the order of 2 yields the reaction orders of water close to zero, and high SC gives negative values [67].

The concentration of the different gases in the anode and fuel channel (only the water-gas shift reaction, r_s) is changing as the above described reactions proceed as:

$$r_{CH_4} = -r_r \quad (25)$$

$$r_{H_2} = 3 \cdot r_r + r_s \quad (26)$$

$$r_{CO} = r_r - r_s \quad (27)$$

$$r_{CO_2} = r_s \quad (28)$$

$$r_{H_2O} = -r_r - r_s \quad (29)$$

where r_i is the reaction rate of species i . The catalytic steam reforming is expressed by r_r and the water-gas shift reaction by r_s .

Chapter 3

Mathematical models

A two-dimensional model for an anode-supported SOFC is developed and implemented in the commercial software COMSOL Multiphysics (version 3.5). Equations for momentum-, mass- and heat transport are solved simultaneously. A sketch of the modeled cell can be seen in Fig. 6 and the geometry is defined in Table 4. Note the difference in scale between the cell length (x -direction, as in Fig. 6) and various thicknesses (y -direction, as in Fig. 6). It should be mentioned that the model in this study is 2D only, and the connection between the electrodes and interconnect can not be explicitly observed in this case.

Two approaches for defining the electrochemical reactions can be found in the literature, either as source terms in the governing equations [40, 51] or as interface conditions defined at the electrode/electrolyte interfaces [31, 49, 68-71]. The electrochemical reactions in the model presented in this chapter defined as interface conditions, and this approach affects the momentum-, heat transfer- and mass transport equations. This approach can be used, because the thickness of the active layer is sufficiently thin, compared to the thickness of the electrode [31, 49, 68-71]. The reason for using an approach where the electrochemical reactions are defined as source terms is that the reaction zone can be spread out into the electrode some distance away from the electrode/electrolyte interface [40].

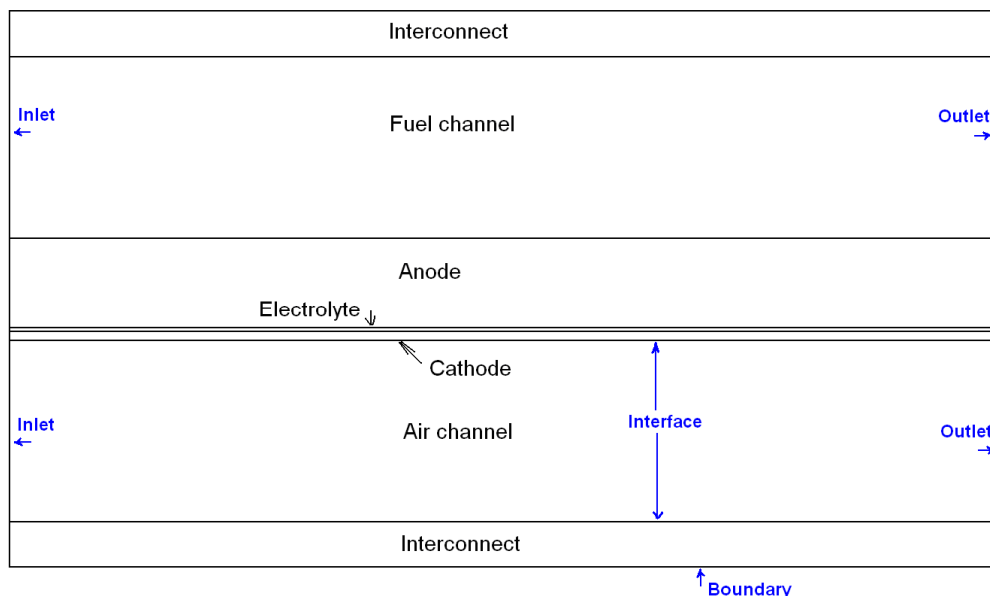


Figure 6: Sketch of an anode-supported SOFC, not to scale.

Table 4. Cell geometry [72].

<i>Cell length</i>	0.4 m
<i>Fuel channel height</i>	1 mm
<i>Air channel height</i>	1 mm
<i>Anode thickness</i>	500 μm
<i>Cathode thickness</i>	50 μm
<i>Electrolyte thickness</i>	20 μm
<i>Interconnect thickness</i>	500 μm

Oxygen is reduced in the cathode (eqn. (30)), and the generated oxygen ions migrate through the electrolyte and then react with hydrogen in the anode (eqn. (31)) [53].



The surplus of oxygen is specified as:

$$S_{O_2} = \frac{x_{O_2,0}}{x_{O_2,0} - x_{O_2,end}} - 1 \quad (32)$$

where x_{O_2} is the molar fraction of oxygen, 0 stands for inlet and end is outlet. The consumption of fuel is specified as:

$$C_{fuel} = \frac{x_{H_2,0} - x_{H_2,end}}{x_{H_2,0}} \quad (33)$$

3.1 Assumptions

The assumptions being made are described throughout the text related to their respective equations or chapters and outlined as follows:

- The developed model is in two dimensions, as shown in Fig. 6 and explained in chapter 3.
- The electrochemical reactions are specified at the electrolyte/electrode interfaces and not as source terms in the electrodes, as explained in chapter 3.
- The Knudsen diffusion term is neglected (3.2.2).
- The temperature distribution is calculated separately for the gas- and solid phases, (3.2.3 and 3.3.3).
- The entry effects on the flow profile are neglected (3.3.1)
- A gas velocity effect is calculated to include the electrochemical reactions effects on the momentum transport equations (3.3.1).
- The Nusselt number is assumed to be constant (3.3.3).
- The changes in entropy and enthalpy due to the chemical reactions are defined at a constant temperature only (3.3.3 and 3.4).
- The thermal conductivity and heat capacity for the solid parts are assumed to be temperature independent in the temperature range used in this work (4).
- An average current density is defined as a constant (4).

3.2 Governing equations

3.2.1 Momentum equation

The gases flow inside the fuel cell components, such as in the air and fuel channels and to the porous electrodes. A traditional modeling approach for such a system consists of solving the Darcy's equation in the porous medium and the Navier-Stokes equations in the channels separately. The problem with such an approach is to define interface conditions at the interface between the two domains. It is hard to define this tangential velocity component. To avoid this problem the Darcy-Brinkman equation is introduced and solved for the gas flow in the fuel and air channels and in the porous media (electrodes) [54, 73].

The Darcy-Brinkman equation (eq. (34)) is transformed into the standard Navier-Stokes equation when ($\kappa \rightarrow \infty$) and ($\varepsilon_p = 1$), and into the Darcy equation as ($Da \rightarrow 0$), Da is the Darcy number. The derivation of Navier-Stokes equation and Darcy equation from Darcy-Brinkman equation can be found in [54].

$$\left(\frac{\mu}{\kappa} + \rho \cdot \nabla \mathbf{u} \right) \mathbf{u} - \nabla \left[-p + \frac{1}{\varepsilon_p} \{ \mathbf{T} - (\lambda - \kappa_{dv})(\nabla \mathbf{u}) \} \right] = \mathbf{F} \quad (34)$$

where \mathbf{F} is the volume force vector, κ is the permeability of the porous medium, ε_p the porosity, μ the dynamic viscosity, \mathbf{u} the velocity vector and \mathbf{T} the viscous stress tensor ($\mathbf{T} = \nu(\nabla \mathbf{u} + (\nabla \mathbf{u})^T)$). κ_{dv} (deviation from thermodynamic equilibrium) is by default set to zero, which means that the fluid particles are in equilibrium with their surrounding. λ is the second viscosity and is, for gases, normally assumed as: $\lambda = -2/3 \mu$ [37]. The equation for the continuity in the air and fuel channels reads: $\nabla \cdot \mathbf{u} = 0$ [73]. The densities for the participating gases are calculated as [73]:

$$\rho_{mixture} = \frac{p \cdot \sum x_i \cdot M_i}{R \cdot T} \quad (35)$$

The dynamic viscosity for each participating species in the gas phase is calculated as [74]:

$$\mu_i = \sum_{k=1}^7 b_k \cdot \left(\frac{T}{1000} \right)^k \quad (36)$$

where b_k is the species dependent parameter and “k” stands for the number of species dependent parameters in the viscosity equation. The dynamic viscosity for the gas mixtures is calculated as [74]:

$$\mu_{mixture} = \sum x_i \cdot \mu_i \quad (37)$$

3.2.2 Mass transport equation

The Maxwell-Stefan equation for mass diffusion and convection is used to describe the mass transport phenomena for the gases inside the fuel cell [73]. The Maxwell-Stefan equation is a simplified equation compared to “Dusty Gas Model”, since the Knudsen diffusion (collisions between gas molecules and the porous material) is neglected. The reason for this treatment is to reduce the calculation cost and this model is already predefined in the commercial software COMSOL Multiphysics, that is used in this work. However, adding the Knudsen diffusion term

may increase the diffusion resistance. The Maxwell-Stefan equation is solved for the fuel and air channels and electrodes.

$$\nabla \left(-\rho \cdot w_i \sum \bar{D}_{ij} \cdot \nabla x_j + (x_j - w_j) \frac{\nabla p}{p} \cdot \mathbf{u} - D_i^T \cdot \frac{\nabla T}{T} \right) + \rho \cdot \mathbf{u} \cdot \nabla w_j = S_i \quad (38)$$

$$x_j = \frac{w_j}{M_j} \cdot M \quad (39)$$

$$\sum_{i=1}^n w_i = 1 \quad (40)$$

where w is the mass fraction, x the mole fraction, n the number of species, D_i^T the thermal diffusion coefficient and D_{ij} the Maxwell-Stefan binary diffusion coefficient. S_i , the reaction rate, is zero in this case because the electrochemical reactions are assumed to take place, as mentioned, at the interfaces between the electrolyte and electrodes. The electrochemical reactions occur in reality at an active reaction surface area, the three phase boundary, where gas, ionic and electronic phases meet. The active reaction surface area will be considered in future research as the electrochemical reactions are defined as source terms in the mass transport governing equation instead as interface conditions, as discussed before. The diffusion coefficient in the porous electrodes is calculated as [50, 75]:

$$D_{ij,por} = D_{ij} \cdot \varepsilon_p / t \quad (41)$$

where t is the tortuosity and D_{ij} is calculated as [76]:

$$D_{ij} = \frac{2.66 \cdot 10^{-8} \cdot T^{3/2}}{p \cdot M_{ij}^{1/2} \cdot l_{ij}^2 \cdot \Omega_D} \quad (42)$$

$$\Omega_D = \frac{A}{\left(\frac{k'T}{e_{ij}} \right)^B} + \frac{C}{\exp\left(D \cdot \frac{k'T}{e_{ij}} \right)} + \frac{E}{\exp\left(F \cdot \frac{k'T}{e_{ij}} \right)} + \frac{G}{\exp\left(H \cdot \frac{k'T}{e_{ij}} \right)} \quad (43)$$

$$M_{ij} = \frac{2}{\frac{1}{M_i} + \frac{1}{M_j}} \quad (44)$$

$$l_{ij} = \frac{l_i + l_j}{2} \quad (45)$$

$$e_{ij} = \sqrt{e_i \cdot e_j} \quad (46)$$

where Ω_D is the diffusion collision integral, e_{ij} the average characteristic Lennard-Jones energy, l_{ij} the average characteristic length, M_{ij} the average molecular weight, and k' the Boltzmann's constant. A, B, C, D, E, F, G and H are constants, as shown in [76].

3.2.3 Heat transfer equation

The temperature distribution is calculated separately for the gas phase (in air and fuel channels and electrodes) and for the solid phase (interconnect, electrodes and electrolyte). Heat is transferred between the phases at the channel walls and in the porous electrodes. The general heat conduction equation is used to calculate the temperature distribution for the solid materials, i.e., electrolyte, interconnect and electrodes [73]:

$$\nabla(-k_s \cdot \nabla T_s) = Q_s \quad (47)$$

where k_s is the thermal conductivity of the solids, T_s the temperature in the solid phase and Q_s the heat source (heat transfer between the solid and gas phases and heat generation due to ohmic polarization). Note that heat generated due to ohmic polarization is assumed to enter the solid phase (as a part of Q_s), heat generation due to electrochemical reactions, concentration and activation polarization are simplified and defined as interface conditions, as for the mass transport. The temperature distribution for the gas mixtures in the fuel and air channels and in the porous electrodes is calculated as [73]:

$$\nabla(-k_g \cdot \nabla T_g) = Q_g - \rho_g \cdot c_{p,g} \cdot \mathbf{u} \cdot \nabla T_g \quad (48)$$

where $c_{p,g}$ is the gas phase heat capacity, T_g the temperature in the gas phase and Q_g the heat transfer between the gas and solid phases. Because the Reynolds number is very low, the heat transfer coefficient ($h_{s,g,por}$) in the porous electrodes (when assumed spherical particles in the porous electrodes) can be calculated as [57]:

$$h_{s,g,por} = \frac{2 \cdot k_g}{d_p} \quad (49)$$

where d_p is the electrode particle diameter and k_g the gas conductivity. The heat transfer between the gas phase and solid phase depends on the temperature difference and the particle surface area as [77]:

$$Q_g = h_v \cdot (T_g - T_s) = SA \cdot h_{s,g,por} \cdot (T_g - T_s) \quad (50)$$

where h_v is the volume heat transfer coefficient and SA the surface area (760 000 m²/m³ for the cathode and 619 000 m²/m³ for the anode [78]). The temperature difference between the solid and gas phases has been found to be negligible (the average temperature difference is 5.5 · 10⁻⁴ K for the cathode and 9.8 · 10⁻⁶ K for the anode) for the situation considered in this study. This small temperature difference between the solid and gas phase in the porous electrodes is due to the big surface area and very small particle diameter assumed in this study. As a comparison it can be mentioned that the temperature difference between the gas and solid phase in [57] was in the order of 10⁻² K. The average heat transfer (Q_g) between the phases are 3.5 · 10⁶ in the anode and 6.2 · 10⁷ W/m³ in the cathode, compared to the maximum value, 7.5 · 10⁹ W/m³ in the anode and 7.1 · 10⁹ W/m³ in the cathode. The big difference between average and maximum heat transfer values is due to the large surface area.

A parameter study is made, as shown in Table 5, to study the temperature difference between the solid and gas phases when surface area and the heat transfer coefficient (between the gases and the (solid) walls) are varied. It is found that the surface area has a big influence on the temperature difference between the solid and gas phases. The temperature difference changes in the same order as the surface area does

Table 5. LTNE parameter study for the phase temperature difference.

	Anode		Cathode	
	average	maximum	average	maximum
<i>Basic case [K]</i>	$9.8 \cdot 10^{-6}$	0.014	$5.5 \cdot 10^{-4}$	0.067
<i>SA*10 [K]</i>	$1.1 \cdot 10^{-6}$	$1.4 \cdot 10^{-3}$	$6.0 \cdot 10^{-5}$	$7.6 \cdot 10^{-3}$
<i>SA/10 [K]</i>	$5.8 \cdot 10^{-5}$	0.13	$5.2 \cdot 10^{-3}$	0.34
$h_{sg,cb} * 2 [K]$	$9.8 \cdot 10^{-6}$	0.014	$5.4 \cdot 10^{-5}$	0.065
$h_{sg,cb} / 2 [K]$	$9.8 \cdot 10^{-6}$	0.015	$5.5 \cdot 10^{-4}$	0.069

The heat capacity for each gas species is calculated as [74]:

$$c_{p,i}(T) = \sum_{k=1}^7 a_k \cdot \left(\frac{T}{1000} \right)^k \quad (51)$$

where a_k is the species dependent parameter (extracted from [74]) and “k” stands for the number of parameters in the heat capacity equation. The heat capacities for the gas mixtures can then be calculated when the individual species values are known [74]:

$$c_{p,mixture} = \sum x_i \cdot c_{p,i} \quad (52)$$

The gas thermal conductivity for each species in the gas phase is calculated as [74]:

$$k_{g,i}(T) = 0.01 \cdot \sum_{k=1}^7 c_k \cdot \left(\frac{T}{1000} \right)^k \quad (53)$$

where c_k is the species dependent parameter (extracted from [74]) and “k” stands for the number of parameters in the thermal conductivity equation. The conductivity for the gas mixtures can then be evaluated as [74]:

$$k_{g,mixture} = \sum x_i \cdot k_{g,i} \quad (54)$$

Ohmic polarization occurs due to resistance of the flow of ions in the electrolyte and electrical resistance in the electrodes. The electrodes and electrolyte are heated due to this effect [5, 79]:

$$Q_{ohm} = \frac{i \cdot \eta_{ohm}}{\tau} \quad (55)$$

$$\eta_{ohm} = R_{ohm} \cdot i \quad (56)$$

$$R_{ohm} = \frac{\tau_a}{\sigma_a} + \frac{\tau_{el}}{\sigma_{el}} + \frac{\tau_c}{\sigma_c} \quad (57)$$

where τ is the component thickness and R_{ohm} the electrolyte area-specific ohmic resistance. The electron/ionic conductivities (σ) are calculated as [5, 71]:

$$\sigma_a = \frac{4.2 \cdot 10^7}{T} \cdot \exp\left(\frac{-1200}{T}\right) \quad (58)$$

$$\sigma_{el} = 33.4 \cdot 10^3 \cdot \exp\left(\frac{-10300}{T}\right) \quad (59)$$

$$\sigma_c = \frac{9.5 \cdot 10^7}{T} \cdot \exp\left(\frac{-1150}{T}\right) \quad (60)$$

3.3 Boundary and interface conditions

3.3.1 Momentum transport

The boundary conditions for the momentum transport equation are defined as a laminar flow profile for the inlet with an average air inflow velocity of 5.2 m/s (for an oxygen surplus factor of 4). The entrance length due to the build up of a fully developed velocity profile can be neglected since the channel length is 400 times bigger than its height. The outlet is defined as [73]:

$$\mu(\nabla \mathbf{u} + (\nabla \mathbf{u})^T) \cdot \mathbf{n} = 0 \quad (61)$$

$$p = p_0 \quad (62)$$

where p_0 is a defined outlet pressure (=1 atm). The interfaces between the interconnects and gas channels have to be defined since the governing equation for momentum transport is not solved for the interconnects, the interfaces are defined as walls ($\mathbf{u}=0$). The Darcy-Brinkman equation makes it possible to define the interface between the air and fuel channels and the porous electrodes as continuous. The Darcy-Brinkman equation is not solved for the electrolyte and the interface conditions need to be defined. Oxygen is consumed at the interface between the cathode and electrolyte, and the electrochemical reaction rate depends on the current density. As for the mass transport, the electrochemical reactions occur in reality at an active reaction surface area, but are in this paper simplified and assumed to occur at the interface between the electrodes and electrolyte. The gas velocity effect (r), calculated from the total mass flow given by the electrochemical reaction, on the momentum equation can be calculated as [73]:

$$r = -\left(\frac{i \cdot M_{O_2}}{n_{e,c} \cdot F \cdot \rho}\right) \quad (63)$$

where i is the current density and $n_{e,c}$ the number of electrons transferred per molecule of oxygen consumed (= 4). At the anode and electrolyte interface one molecule of water is produced for every molecule of hydrogen consumed, and the reaction effect is specified as [73]:

$$r = \frac{i \cdot (M_{H_2O} - M_{H_2})}{n_{e,a} \cdot F \cdot \rho} \quad (64)$$

where $n_{e,a}$ the number of electrons transferred per molecule of hydrogen consumed/water produced (= 2). The implementation of eq. (63) and (64) means that the cell overall mass balances is very good.

3.3.2 Mass transport

The boundary conditions for the mass transport equation are defined as mass fractions at the gas channel inlet ($w_i = w_{i,0}$) and the boundaries. However, the result can be presented as either mass or mole fraction. The convective flux for the gas channel outlet is defined as [73]:

$$\mathbf{n} \cdot \left(-\rho \cdot w_i \sum D_{ij} \left(\nabla x_j + (x_j - w_j) \cdot \frac{\nabla p}{p} \right) - D^T \frac{\nabla T}{T} \right) = 0 \quad (65)$$

The flows from the anode and the cathode to the electrolyte are defined as “flux” [73]:

$$-\mathbf{n} \cdot \mathbf{N} = n_0 \quad (66)$$

$$\mathbf{N} = -\rho \cdot w_i \sum D_{ij} \left(\nabla x_j + (x_j - w_j) \cdot \frac{\nabla p}{p} \right) + D^T \cdot \frac{\nabla T}{T} + \rho \cdot w_i \cdot \mathbf{u} \quad (67)$$

where \mathbf{n} stands for the normal vector to the boundary, and n_0 for the inward mass flux [73]:

$$n_0 = \frac{-i \cdot M_i}{n_e \cdot F} \quad (68)$$

where i is the current density and n_e the number of electrons transferred per reaction, and F the Faraday constant. The interfaces between the interconnects and the gas channels have to be defined because the governing equation for mass transport is not solved for the interconnects.

3.3.3 Heat transfer

As described previously (in chapter 3.2.3) the temperature in the solid and gas phase is calculated separately. The inlet gas temperature is defined by the operating conditions. The outlet for the gas channels is defined as a convective flux [73]:

$$-\mathbf{n} \cdot (-k \cdot \nabla T_g) = 0 \quad (69)$$

The boundaries at the top and bottom of the model are defined as symmetry, because it is assumed that the cell is surrounded by other cells with the same temperature distribution. The heat flux at the interface between the interconnects and gas channels as well as at the interface between the gas channels and electrodes is defined as [73]:

$$-\mathbf{n} \cdot (-k_s \cdot \nabla T_s) = q_s \quad (70)$$

$$q_s = h_{s,g,cb} \cdot (T_s - T_g) \quad (71)$$

$$q_g = -q_s \quad (72)$$

where T_s is the temperature in the solid phase, T_g the temperature in the gas phase, q_g is the heat flux from the gas phase, q_s the heat flux to the solid phase and $h_{s,g,cb}$ the heat transfer coefficient between the gases and the (solid) walls [80]:

$$h_{s,g,cb} = \frac{Nu \cdot k_g}{d_c} \quad (73)$$

where Nu is Nusselt number, k_g gas phase conductivity and d_c the channel diameter (=1 mm). The value for Nusselt number (4.094) comes from [80], based on the fully developed flow for a rectangular duct (aspect ratio is 1 for both channels). The heat flux is specified at two channel walls, located opposite to each other. One is located between the interconnect and the gas channel, and another one is between the electrode and gas channel. Heat generated due to

electrochemical reactions and due to polarization losses are, as previously described, defined at the electrodes/electrolyte interfaces:

$$-n \cdot (-k \cdot \nabla T) = q_0 \quad (74)$$

$$q_0 = q_r + q_{losses} = -i \cdot \left(\frac{T \cdot \Delta S_r}{n_e \cdot F} + \eta_{act,e} + \eta_{conc,e} \right) \quad (75)$$

where q_0 is the heat generated at the interface (specified as interface condition), q_r the heat generated inside the cell due to change in enthalpy and q_{losses} the heat generated due to potential losses inside the cell. It is assumed that this heat (q_0) is generated in the gas phase. The amount of heat due to electrochemical reactions can be calculated as [53, 58]:

$$q_r = -T \cdot \Delta S_r \cdot \dot{n} = -\Delta S_r \frac{T \cdot i}{n_e F} \quad (76)$$

$$\dot{n} = \frac{i}{n_e F} \quad (77)$$

where \dot{n} is the molar flux density [mol/(m²s)] and ΔS_r entropy change of the reaction [-50.2 J/(K mol)], calculated from data in [81]. The heat generation due to the activation and the concentration polarization can be calculated as [50, 79]:

$$q_{losses} = -i \cdot (\eta_{act,e} + \eta_{conc,e}) \quad (78)$$

The concentration polarizations due to the concentration differences inside the cell are specified as [5]:

$$\eta_{conc,a} = \frac{R \cdot T}{n_{e,a} \cdot F} \cdot \ln \left(\frac{p_{H_2O,TPB} \cdot p_{H_2,b}}{p_{H_2,TPB} \cdot p_{H_2O,b}} \right) \quad (79)$$

$$\eta_{conc,c} = \frac{R \cdot T}{n_{e,c} \cdot F} \cdot \ln \left(\frac{p_{O_2,b}}{p_{O_2,TPB}} \right) \quad (80)$$

where $p_{i,TPB}$ stands for the partial pressure at three phase boundary (TPB) and $p_{i,b}$ the partial pressure at the boundary between the gas channel and the electrode. The chemical reactions involve energy barriers (i.e., the activation polarization) which must be overcome by the reacting species. The activation polarization can be considered as the extra potential needed to overcome the energy barrier of the rate-determining step to a value that the reaction proceeds at a desired rate. It is normally expressed by the Butler-Volmer equation [50]:

$$i = i_0 \left\{ \exp \left(\beta \cdot \frac{n_e \cdot F \cdot \eta_{act,e}}{R \cdot T} \right) - \exp \left(-(1 - \beta) \frac{n_e \cdot F \cdot \eta_{act,e}}{R \cdot T} \right) \right\} \quad (81)$$

where β is the transfer coefficient, usually assumed to be 0.5. The Butler-Volmer equation can then be expressed as [5, 50]:

$$i = 2 \cdot i_0 \cdot \sinh \left(\frac{n_e \cdot F \cdot \eta_{act,e}}{2 \cdot R \cdot T} \right) \quad (82)$$

$$\eta_{act,e} = \frac{2 \cdot R \cdot T}{n_e \cdot F} \sinh^{-1} \left(\frac{i_e}{2 \cdot i_{0,e}} \right) \quad (83)$$

$$i_0 = \frac{R \cdot T}{n_e \cdot F} k''_e \cdot \exp \left(\frac{-E_e}{R \cdot T} \right) \quad (84)$$

where i_0 is the exchange current density. The pre-exponential factor (k'') is $2.35 \cdot 10^{11} \Omega^{-1} \text{m}^{-2}$ for the cathode and $6.54 \cdot 10^{11} \Omega^{-1} \text{m}^{-2}$ for the anode, respectively. The activation energy (E) is 137 kJ/mol for the cathode and 140 kJ/mol for the anode [5, 42].

3.5 Extended model considering internal reforming reactions

The basic model is extended to include the reforming reactions, hydrogen, water, methane, carbon monoxide and carbon dioxide are considered at the fuel side. The cell geometry is as for the basic model, besides the cell length is shortened to 0.1 m to limit the calculation time. The flow rates in the air and fuel channels are reduced (in comparison to the basic model) to have the same oxygen surplus factor and consumption of fuel, specified as:

$$C_{fuel} = \frac{x_{fuel,0} - x_{fuel,end}}{x_{fuel,0}} \quad (85)$$

$$x_{fuel} = x_{H_2} + x_{CO} + 4 \cdot x_{CH_4} \quad (86)$$

where C_{fuel} is the consumption of fuel and x_i the mole fraction of molecule i . The expression for the fuel mole fraction (x_{fuel}) states that each molecule of carbon monoxide gives one molecule of hydrogen in the water-gas shift reaction and each molecule of methane gives four molecules of hydrogen after the steam reforming reaction and the water-gas shift reaction. The high steam reforming reaction rate (due to the high temperature) converts the methane into hydrogen and carbon monoxide quickly, i.e., the methane in the inlet gas is available as hydrogen in the electrochemical reactions. Note that the mole fraction of water is not a part of the fuel fraction expression, water is needed for both the steam reforming and water-gas shift reforming, and a more advanced expression can be needed for comparison between different fuel mixtures. The fuel mole fraction can theoretically be higher than 1, since each molecule of methane reacts (with water) to 4 molecules of hydrogen.

The Darcy-Brinkman approach, eq. (34), for calculating the flow inside the gas channels and the porous electrodes are used as for the basic case. The density, eq. (35), as well as the dynamic viscosity, eq. (36)-(37), are calculated to include the five gas species mixture on the fuel side. The thermal conductivity (eq. (53)-(54)), is updated to cover the five gas species.

The Maxwell-Stefan equation, eq. (38), is used to calculate the mass distribution within the cell. The reforming chemistry is specified as the source term (S_i) in the governing equation. The equation on the fuel side is updated to consider interactions between the five present gas species (hydrogen, water, methane, carbon monoxide and carbon dioxide). The Maxwell-Stefan diffusion coefficient (D_{ij}) for each two-pair molecule mixture (5 species gives 10 pairs) is calculated according to eq. (42) and then matrix inversion is used to calculate the multicomponent diffusion diffusivity matrix (\bar{D}_{ij}) as [73]:

$$\bar{D}_{ij} = N_{ij} - g \quad (87)$$

where N_{ij} is a matrix that ranges from 1 to the number of components (5), and g is a scalar value that provides numerical stability (should be of the same order in magnitude as the diffusion coefficient) [73].

$$N_{ij} = P_{ij}^{-1} \quad (88)$$

where P_{ij}^{-1} is the inverse of a matrix P_{ij} , as defined in [73]:

$$P_{ij} = \frac{w_i \cdot w_j}{g} - \bar{C}_{ij} \quad (89)$$

where the matrix \bar{C}_{ij} and g are defined as [73]:

$$\bar{C}_{ij} = \begin{cases} \frac{x_i \cdot x_j}{D_{ij}} & i \neq j \\ -\sum_{k \neq j} \bar{C}_{ik} & i = j \end{cases} \quad (90)$$

$$g = \sum_{i=1}^{n-1} \cdot \left(\sum_{j=i+1}^n D_{ij} \right) \quad (91)$$

Note that the multicomponent diffusivity matrix is symmetric, which means that $\bar{D}_{ik} = \bar{D}_{ki}$ [73]. The mass source terms (due to the catalyst reforming reactions) are defined as [51]:

$$S_{H_2} = (3r_r + r_s) \cdot M_{H_2} \quad (92)$$

$$S_{CH_4} = -r_r \cdot M_{CH_4} \quad (93)$$

$$S_{H_2O} = (-r_r - r_s) \cdot M_{H_2O} \quad (94)$$

$$S_{CO} = (r_r - r_s) \cdot M_{CO} \quad (95)$$

The last species (CO_2) can be solved because the sum of the mass fractions equals unity.

Nickel/zirconia is usually used as the material in SOFC anodes, sufficient activity for the steam reforming and the water-gas shift reactions is provided [82]. Reaction kinetics from [51] for the steam reforming and the water-gas shift reactions is used to calculate the reaction velocity, in the anode, in the model developed in this chapter. Other global kinetic models can be found in [60, 66-67, 83-84]. The global reactions for the reforming reaction within the anode are specified as follows [51]:

$$r_r = k_r^+ \cdot p_{CH_4} \cdot p_{H_2O} - k_r^- \cdot p_{CO} \cdot (p_{H_2})^3 \quad (96)$$

$$r_s = k_s^+ \cdot p_{CO} \cdot p_{H_2O} - k_s^- \cdot p_{CO_2} \cdot p_{H_2} \quad (97)$$

where k^+ and k^- are velocity constants of the forward and backward reactions and p is partial pressure. The forward velocity constants are calculated as [51]:

$$k_r^+ = 2395 \cdot \exp(-231266/(R \cdot T)) \quad (98)$$

$$k_s^+ = 0.0171 \cdot \exp(-103191/(R \cdot T)) \quad (99)$$

The backward velocity constants are dependent on the forward velocity constants and the equilibrium constants as [51]:

$$K_{er} = k_r^+ / k_r^- \quad (100)$$

$$K_{es} = k_s^+ / k_s^- \quad (101)$$

The equilibrium constants are functions of the temperature as [51]:

$$K_{er} = 1.0267 \cdot 10^{10} \cdot \exp(-0.2513 \cdot Z^4 + 0.3665 \cdot Z^3 + 0.5810 \cdot Z^2 - 27.134 \cdot Z + 3.27770) \quad (102)$$

$$K_{es} = \exp(-0.2935 \cdot Z^3 + 0.6351 \cdot Z^2 + 4.1788 \cdot Z + 0.3169) \quad (103)$$

$$Z = \frac{1000}{T} - 1 \quad (104)$$

The water-gas shift reaction should be considered to be at equilibrium in the fuel channel. The reaction velocity can be expressed with an equilibrium-limited shift reaction rate expression, first order in carbon monoxide and with arbitrarily high pre-exponential factor as [66]:

$$r_s = k_s \cdot p_{CO} \cdot \left(1 - \frac{p_{CO_2} \cdot p_{H_2}}{K_{e,s} \cdot p_{CO} \cdot p_{H_2O}} \right) \quad (19)$$

where $K_{e,s} = \exp(4276/T - 3.961)$ [66]. The heat generation/consumption due to the reforming reaction is specified in eq. (105) and the enthalpy change due to reaction can be seen in Table 6 [51].

$$Q_{int.ref} = \sum_i R_i \cdot \Delta h_{reaction,i} \quad (105)$$

Table 6. Change in enthalpy for the reforming reactions [51].

	Change in enthalpy (at 1000 K)
<i>Steam reforming reaction</i>	226 kJ/mol
<i>Water-gas shift reaction</i>	-35 kJ/mol

The heat generation/consumption due to the reforming reactions are defined as source terms. Heat generation in the fuel channel (due to water-gas shift reforming reaction) enter obviously in the gas phase. Heat consumption (the steam reforming reaction) and heat generation (the water-gas shift reaction) are assumed to occur on the solid material surface [57]. This assumption is based on the fact that the kinetics for the water-gas shift reaction within the anode is based on characteristics for an SOFC anode with a nickel catalyst. In reality the water-gas shift reaction proceeds both on the solid material surface and in gas phase, however a more detailed kinetic

approach needs to be used to include these phenomena. The heat transfer between the gases and the porous anode structure is very high, (due to the high surface area) and the temperature difference between the phases are found to be very low (as discussed later).

3.6 Numerical methods

All the governing equations were numerically solved in COMSOL Multiphysics (version 3.5) using a stationary solver with a direct (UMFPACK) linear solver system. The residual convergence was limited to 10^{-6} for all variables. Grid independence was achieved at 30 000 finite elements (Fig. 7), after which the change in the maximum temperature was less than 0.1%, change in maximum velocity was less than 1%, oxygen consumption was less than 0.1% and the hydrogen consumption was less than 1% (compared with 53 000 finite elements).

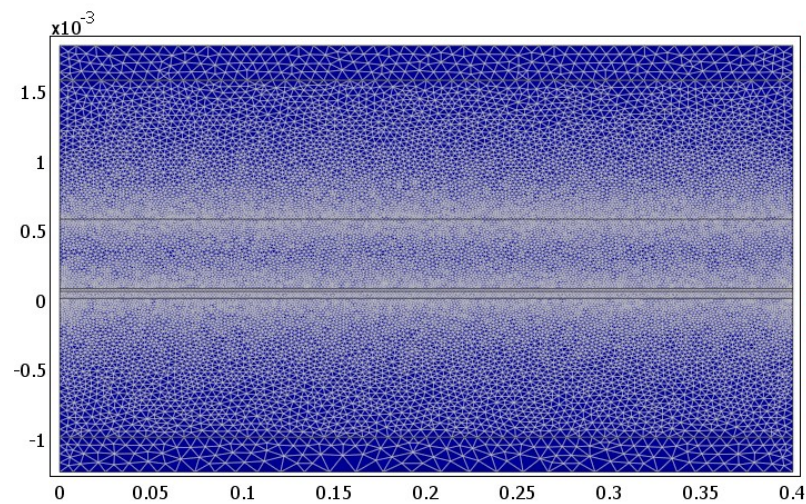


Figure 7: Meshing of the considered geometry for the basic case.

Chapter 4

Results

4.1 Basic model

Material characteristic data typical in the literature are used in this study, as shown in Table 7.

Table 7. Material characteristic data

<i>Anode thermal conductivity, $k_{s,a}$</i>	11 W/m/K	[16]
<i>Cathode thermal conductivity, $k_{s,c}$</i>	6 W/m/K	[16]
<i>Electrolyte thermal conductivity, $k_{s,el}$</i>	2.7 W/m/K	[16]
<i>Interconnect thermal conductivity, $k_{s,int}$</i>	20 W/m/K	[16]
<i>Anode heat capacity, $c_{p,a}$</i>	450 J/kg/K	[65]
<i>Cathode heat capacity, $c_{p,c}$</i>	430 J/kg/K	[65]
<i>Electrolyte heat capacity, $c_{p,el}$</i>	470 J/kg/K	[65]
<i>Interconnect heat capacity, $c_{p,int}$</i>	550 J/kg/K	[65]
<i>Anode solid density, ρ_a</i>	3310 kg/m ³	[65]
<i>Cathode solid density, ρ_c</i>	3030 kg/m ³	[65]
<i>Electrolyte solid density, ρ_{el}</i>	5160 kg/m ³	[65]
<i>Interconnect solid density, ρ_{int}</i>	3030 kg/m ³	[65]
<i>Permeability, κ_e</i>	$1.76 \cdot 10^{11}$ m ²	[16]
<i>Porosity, ε_e</i>	0.5	[16]
<i>Electrode particle diameter, d_p</i>	1 μ m	[75]
<i>Tortuosity, t</i>	5	[75]

A base condition is assumed that the cell average current density is 0.3 A/cm², surplus factor of oxygen is $S_{O_2} = 4$, inlet temperature is 1000 K for both the air and fuel channels and the fuel consumption is $C_{fuel} = 80$ mole-%, and flow direction is left -> right. The above parameters are then varied one by one for parameter studies.

The temperature increases along the x-direction (the main flow direction), as seen in Fig. 9. The temperature difference in the y-direction inside the air channel occurs because the convective heat flux are bigger in the air channel (compared to the fuel channel) due to the relatively larger gas flow rate.

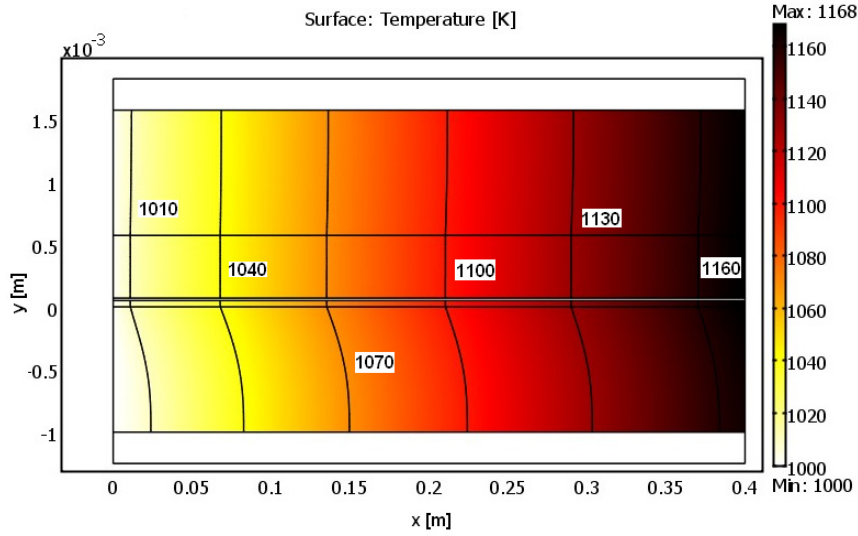


Figure 8: Temperature for the gas phase.

The mole fraction of oxygen (Fig. 9) decreases along the flow direction in the air channel and the cathode. There is a concentration difference in the y-direction as well, that forces the flow towards the cathode/electrolyte interface. However, it is hard to see in the air channel as the cell length is 400 times bigger than the air channel height.

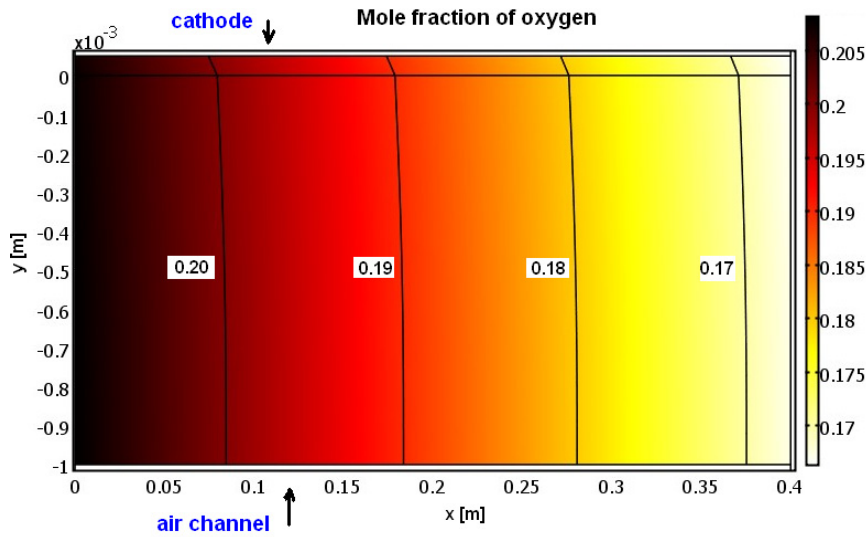


Figure 9: Mole fraction of oxygen in the air channel and cathode

The mole fraction of hydrogen decreases along the flow direction in the fuel channel, as shown in Fig. 10. As for the mole fractions in the air channel, there is a concentration difference in the y-direction for hydrogen, which forces the hydrogen molecules towards the anode/electrolyte interface. However, this effect is very small (impossible to see in the fuel channel), due to the fact that the cell length is 400 times bigger than the fuel channel height.

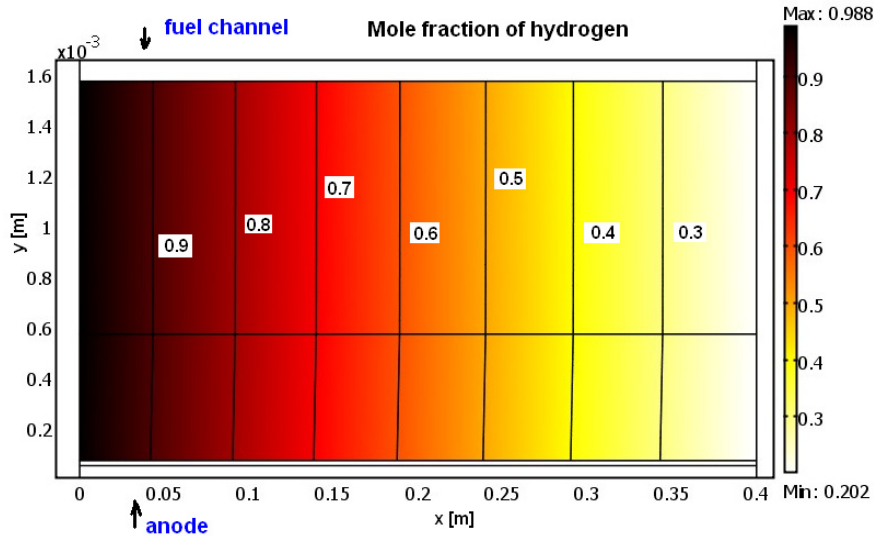


Figure 10: Mole fraction of hydrogen in the fuel channel and anode.

The polarization losses along the flow direction can be seen in Fig. 11. It is found that the ohmic polarizations in the electrodes as well as the concentration polarizations are negligible compared to the activation polarizations and the ohmic polarization in the electrolyte. However, a small effect from concentration polarization is seen in the anode close to the inlet. This effect is not expected as the highest fuel concentration can be found at the inlet. However, the effect on the overall heat balance is found to be negligible. The activation and ohmic polarizations decrease along the flow direction, as the temperature increase (see Fig. 9). It is noted that the activation polarization is more temperature dependent than the ohmic polarization.

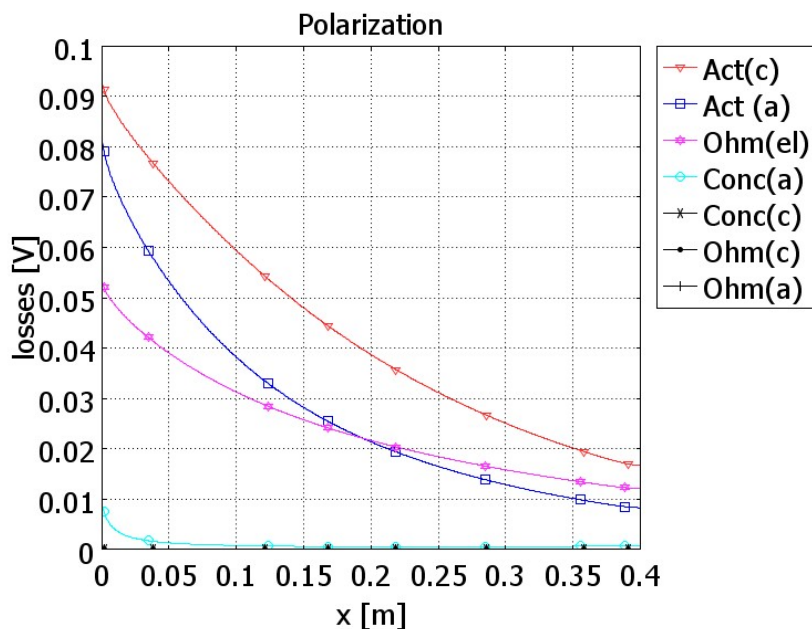


Figure 11: Polarization along the flow direction.

A parameter study is performed to investigate the effect of the oxygen surplus factor, the inlet temperature, the current density, the direction of flow and ionic conductivity. To be able to compare the different investigations with each other, the temperature in the electrolyte is plotted

against the position in the flow direction, except for the case with counter flow, where the temperatures inside the cell are plotted in two dimensions.

A big surplus flow of oxygen cools down the fuel cell, as can be seen in Fig. 12. Change of the oxygen surplus factor is an easy way to control the temperature increase inside the cell, i.e., a higher surplus factor brings a reduced temperature increase along the flow direction. An increased surplus factor also gives a reduced concentration difference in the y -direction, i.e., reduced concentration polarization. However, this effect is found to be negligible in this specific study. A higher surplus of oxygen also means that the energy needed in compressors (driving the air flow in the fuel cell system) will increase.

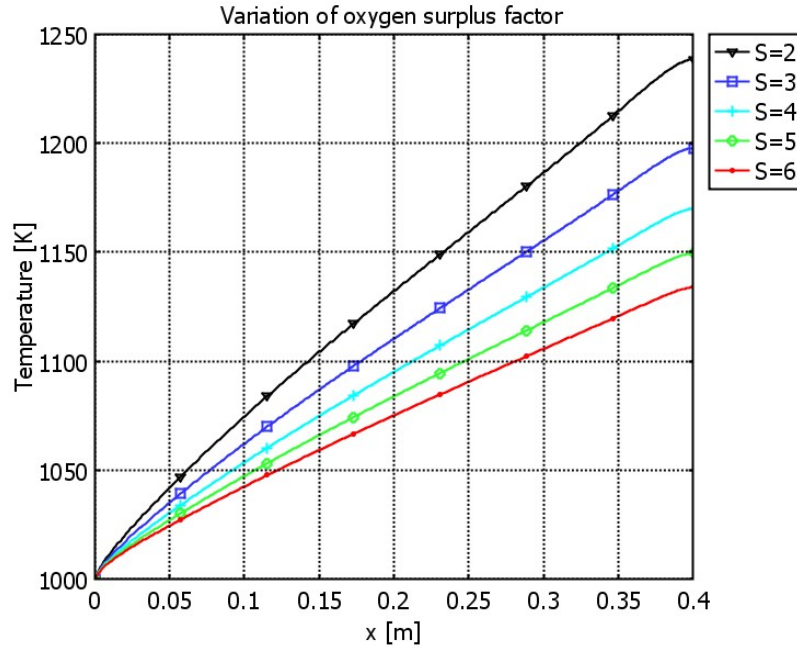


Figure 12: The effect of oxygen surplus factor on temperature along the flow direction in the fuel cell.

An increased inlet temperature gives a reduced temperature increase along the flow direction inside the fuel cell, as can be seen in Fig. 13. This is due to the ohmic heating (ohmic polarization) and the activation polarization (inversed temperature dependence). The ohmic heating decreases with increased inlet temperature because the ionic conductivity in the electrolyte increases. Also the electronic conductivity in the electrodes increases but this effect is found to be much smaller. Both the ionic conductivity and the exchange current density are material dependent, and it is possible to decrease the polarization losses with development of smart suitable materials.

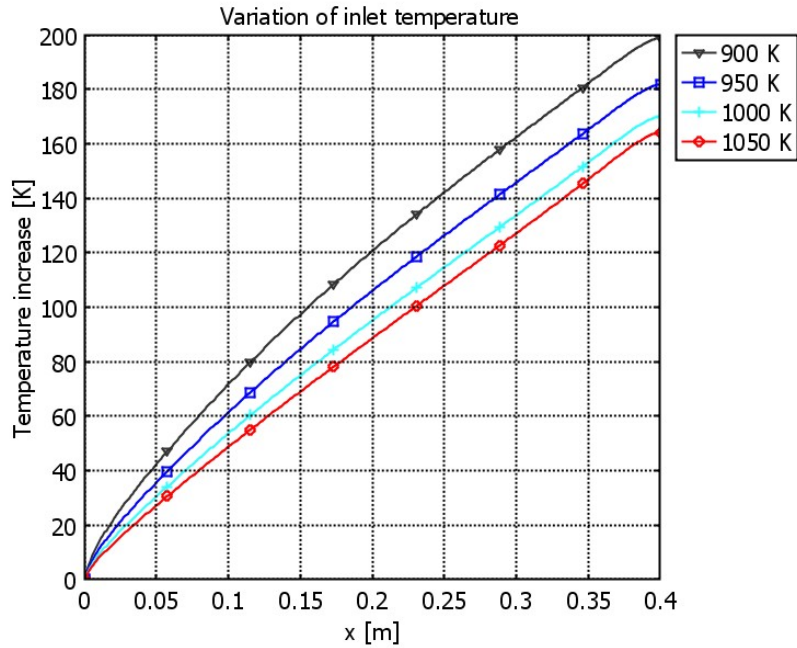


Figure 13: The temperature increase along the flow direction for different inlet temperatures.

The current density influence on the temperature distribution along the flow direction is shown in Fig. 14. An increased current density means that the ohmic and activation polarization increase. A higher current density makes it possible to decrease the fuel cell stack size, however extra heat is produced, due to the increased polarization losses.

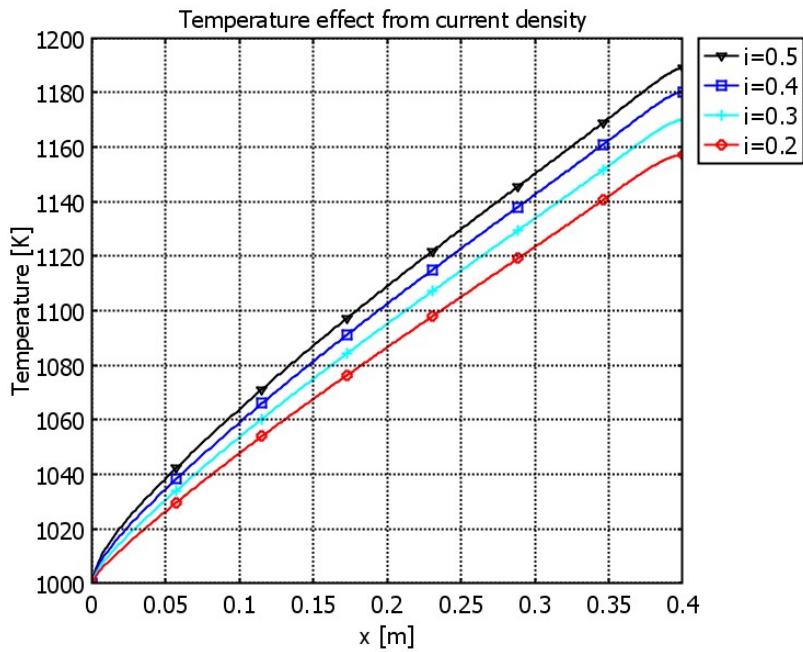


Figure 14: Temperature along the flow direction in the fuel cell for different current densities.

The effect of the ionic conductivity in the electrolyte and the electron conductivity in the electrodes is investigated. A decreased ionic conductivity in the electrolyte makes it harder for the oxygen ions to pass through the electrolyte and the ohmic polarization increases, i.e., the

temperature within the cell increases, as seen in Fig. 15. “50%” means that the ionic conductivity in the electrolyte is halved, and “200%” means that the ionic conductivity is doubled.

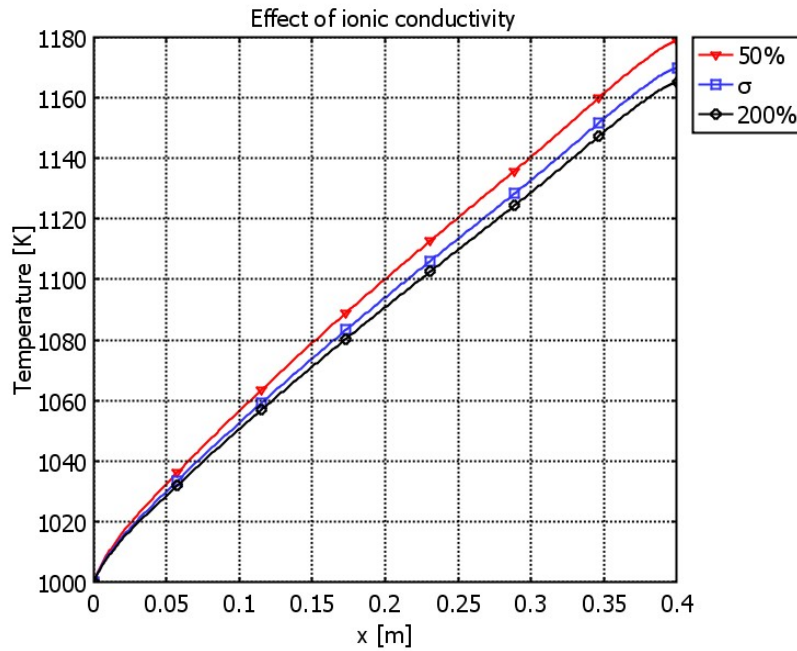


Figure 15: Temperature distribution along the flow direction for different ionic/electronic conductivities.

A simulation is also conducted to study the effect of counter flow, i.e., the air enters into the fuel cell on one side ($x = 0.4$ m) and the fuel from the opposite side ($x = 0$), see Fig. 16. Both the air and fuel gas enter into the cell at 1000 K. The fuel flow is cooled down by the air flow along the channel and the outlet temperature for the fuel gas stream is found to be close to the inlet temperature of the air flow. As the fuel gas stream enters into the cell it is quickly heated up to a temperature close to the outlet temperature of the air flow, and it is expected that this large temperature gradient will cause material problems. It is recommended for counter flow to try to keep the inlet temperature of the fuel stream as close as possible to the outlet temperature of the air stream. Both the temperature gradient inside the cell and the maximum temperature are bigger for a counter flow design, compared to the basic case.

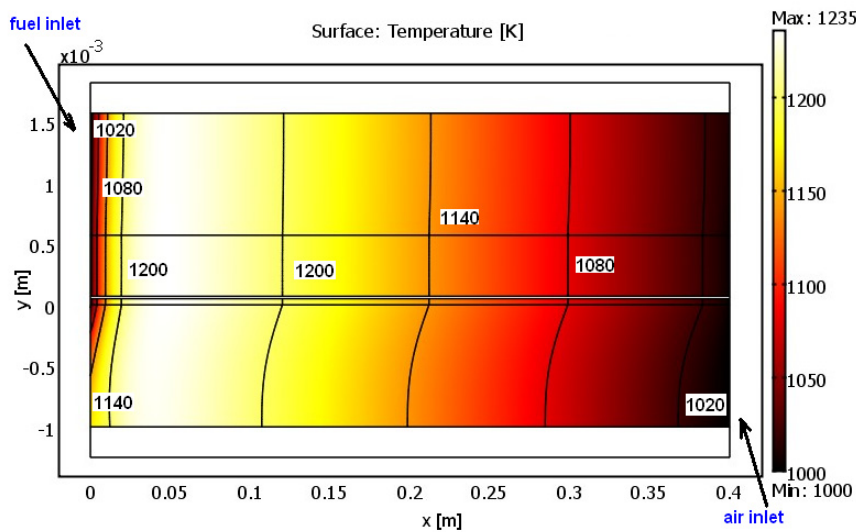


Figure 16: The temperature along the x-axis in count flow

4.2 Model considering internal reforming reactions

The fuel gas inlet conditions are specified as $x_{\text{H}_2} : x_{\text{CH}_4} : x_{\text{CO}} : x_{\text{H}_2\text{O}} : x_{\text{CO}_2} = 0.2626 : 0.171 : 0.0294 : 0.4934 : 0.0436$ (defined by IEA) [67], and the inlet temperature is specified to 1100 K. An average cell current density of 0.3 A/cm^2 , an oxygen surplus factor of 4, fuel consumption of 80 % (mole) and flow direction left \rightarrow right are defined as for the basic case. Material characteristic data can be found in Table 7.

The mole fractions for different gas species in the fuel channel along the flow direction can be seen in Fig. 17. Methane reacts with steam at the Ni-catalyst surface in the porous anode and carbon monoxide and hydrogen is produced. The hydrogen is consumed at the anodic TPB in the electrochemical reactions. The water-gas shift reaction is in equilibrium wherever the gases are present, as hydrogen is consumed and steam generated due to electrochemical reaction the water-gas shift reaction proceeds to the right and more hydrogen is generated.

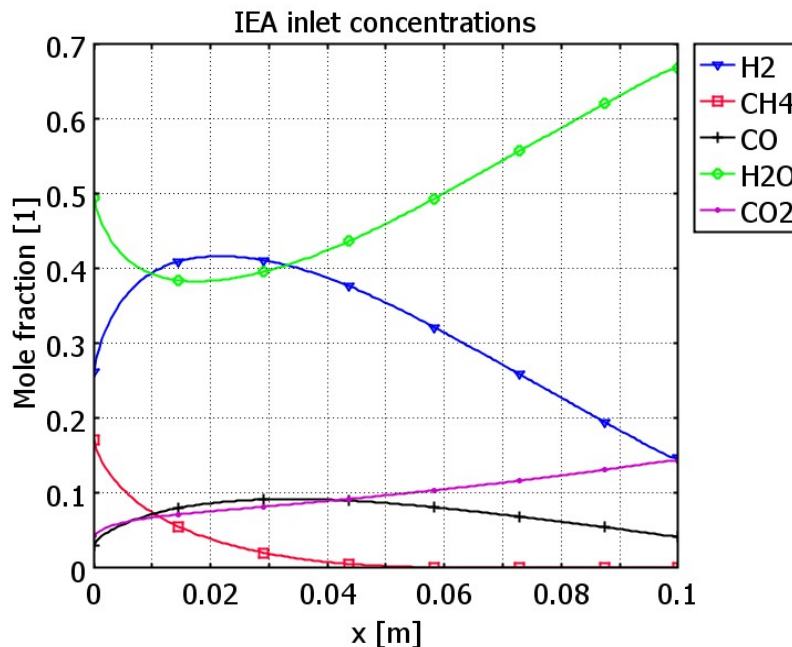


Figure 17: Mole fraction of the gas species in the fuel channel along the flow direction.

The gas-phase temperature within the fuel cell is presented in Fig. 18. The steam reforming reaction decreases the temperature close to the fuel channel inlet. The temperature is slightly lower on the air side (compared to the fuel side), due to a higher air flow rate. The initial temperature decrease is found to be 15 K in the anode, compared 14 K in the cathode, 13 K in the fuel channel and 11 K in the air channel. For the case with higher operating temperature a higher reforming reaction rate is expected and also the temperature close to the inlet decreases faster.

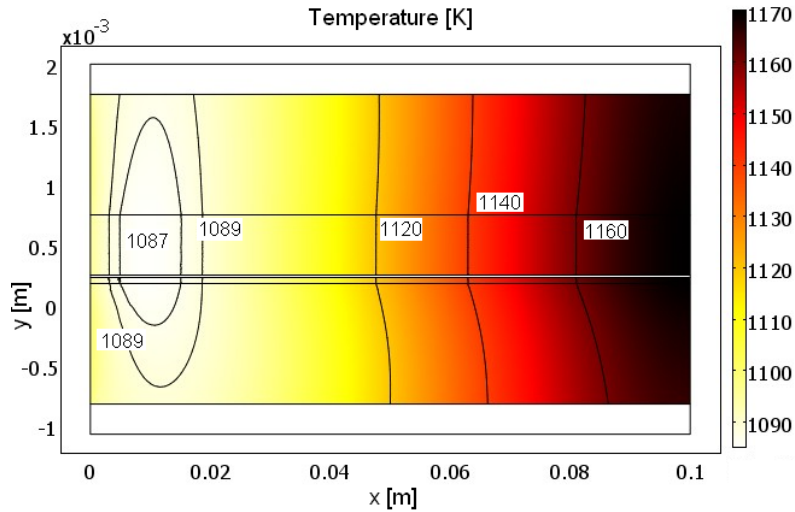


Figure 18: Temperature distribution within the cell in the gas phase.

The mole fraction distribution of methane can be seen in Fig. 19. The concentration difference in the y -direction is due to the consumption of methane in the porous structure. Methane diffuses from the channel towards the porous anode. Note that the fuel channel length is 100 times bigger than the channel height.

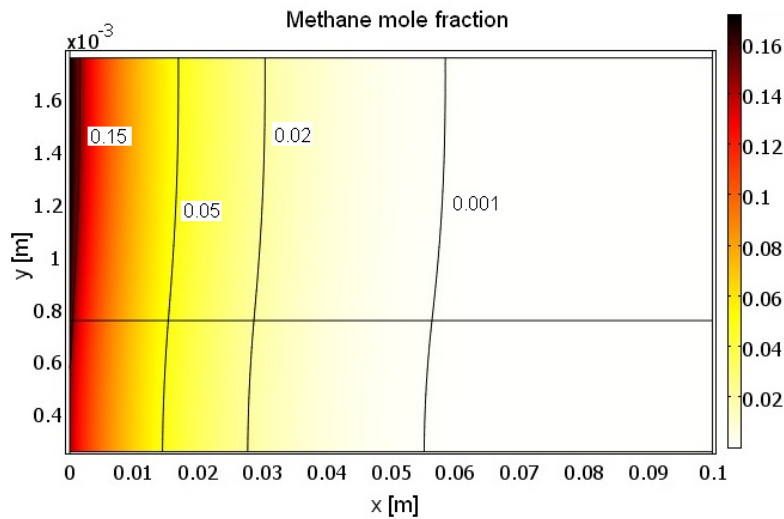


Figure 19: The mole fraction of methane within the anode and fuel channel.

The mole fraction of hydrogen distribution (Fig. 20) increases as the methane and carbon monoxide are catalytically converted into hydrogen. Hydrogen is consumed at the anodic TPB, where the electrochemical reaction takes place. The highest hydrogen concentration along the flow direction can be found where most of the methane is converted. More hydrogen is generated within the cell along the flow direction (thanks to the water-gas shift equilibrium reaction, both in the anode and the fuel channel).

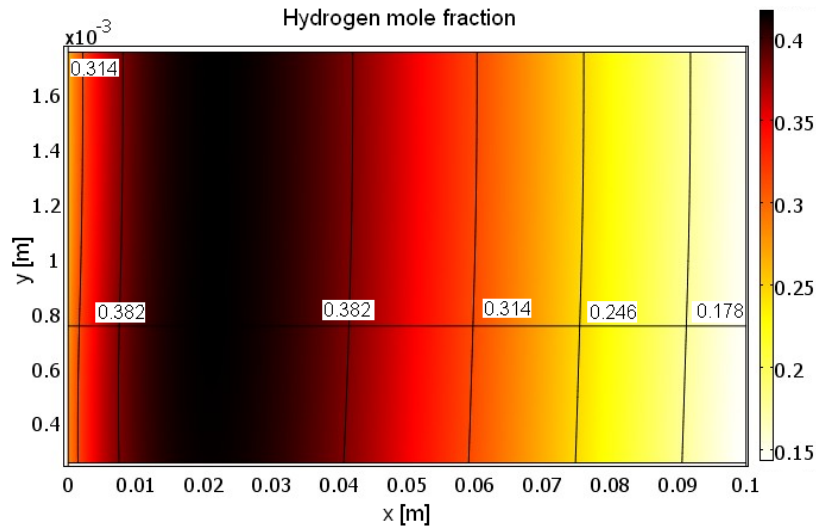


Figure 20: The mole fraction of hydrogen within the anode and fuel channel.

The distribution of carbon monoxide can be seen in Fig. 21. Carbon monoxide is generated within the porous anode structure as the methane is reformed, and then gradually converted to hydrogen and carbon dioxide, due to the water-gas shift equilibrium reaction. The concentration difference in the y -direction close to the inlet is because the methane reforming takes only place in the anode (and not in the fuel channel). The highest concentration can be found after all methane is reformed. Carbon monoxide can participate in the electrochemical reactions, but in this study it is assumed that it is first converted to hydrogen in the water-gas shift reaction.

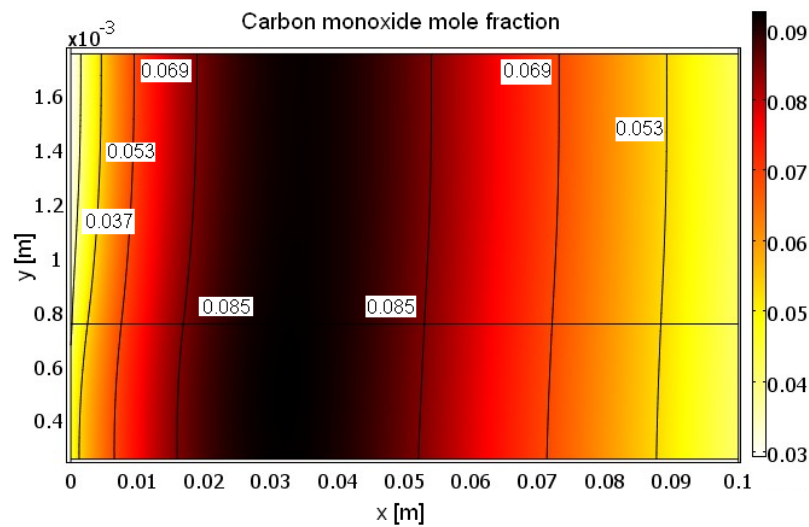


Figure 21: The mole fraction of carbon monoxide within the anode and fuel channel.

The reaction rate for the steam reforming reaction is high close to the inlet where the concentration of methane is high. The reforming reaction proceeds in the anode at the catalytic nickel surfaces. All the anode depth is used for reaction, as can be seen in Fig. 22.

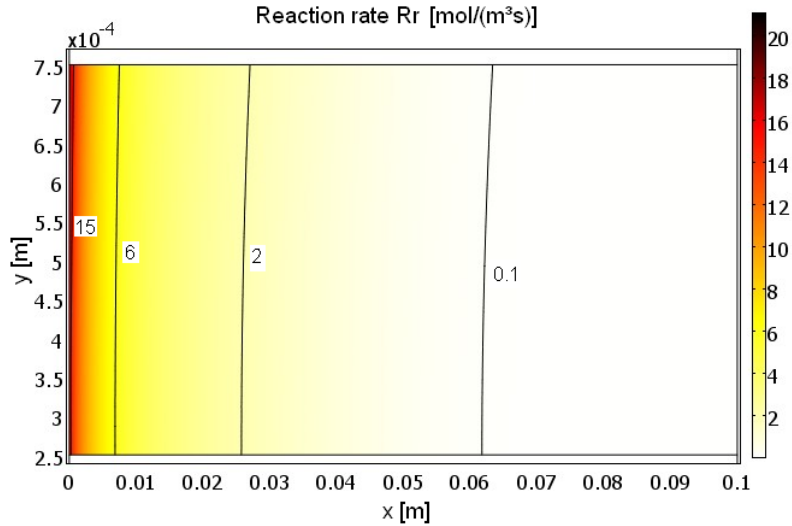


Figure 22: Reaction rate for the steam reforming reaction within the anode.

The reaction rate for the water-gas shift reforming reaction (Fig. 23) is highest in the anode close to the fuel channel inlet where the generation of carbon monoxide is high, due to the steam reforming reaction. The water-gas shift reaction proceeds in the anode at the catalytic nickel surfaces as well as in the fuel channel. As hydrogen is consumed and steam generated due to electrochemical reaction the water-gas shift reaction proceeds to the right and more hydrogen is generated.

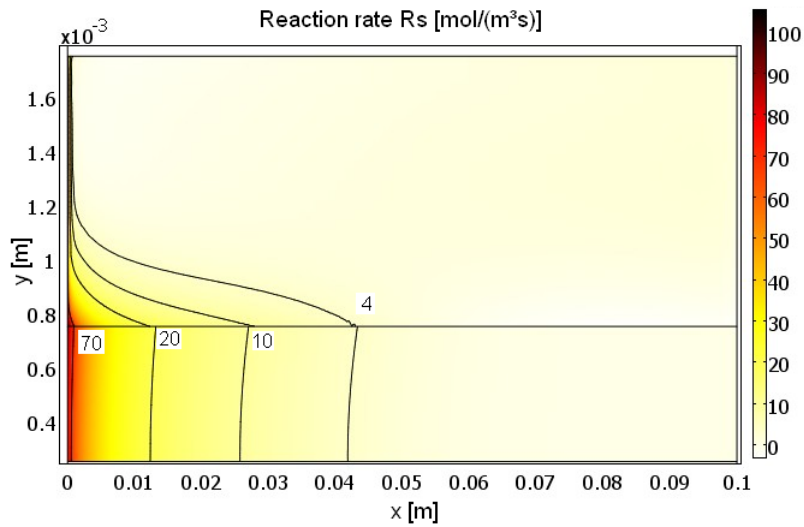


Figure 23: Reaction rate for the water-gas shift reaction within the anode and fuel channel.

The reaction velocity for the steam reforming reaction depends on the temperature, concentrations, catalyst loading and the design of the porous material among other things. The inlet temperature is varied in Fig. 24 to study its effect on the steam reforming velocity (methane mole fraction). A higher operating temperature means higher reaction velocities (sharp decrease in methane mole fraction) and also a decrease in temperature close to the inlet, due to the endothermic steam reforming. Note that an inlet temperature of 1050 K is enough with the assumptions used in this study for all the methane (>99%) to be reformed to hydrogen and carbon monoxide.

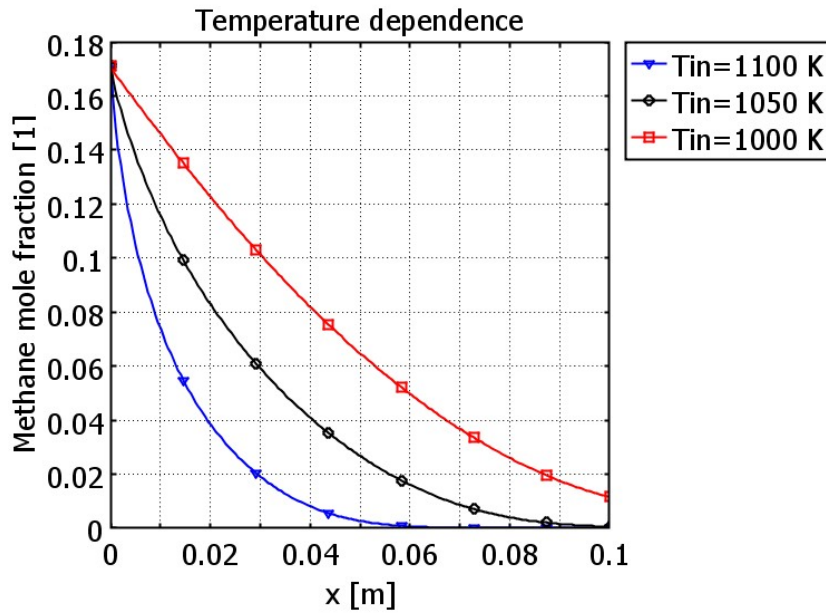


Figure 24: Methane mass fraction in the fuel channel along the flow direction.

The plots in Fig. 25 show that usage of a hydrocarbon fuel (same mole fractions as in Fig. 17) decreases the temperature inside the FC, compared to the case when only hydrogen is used as fuel. Lowering the temperature inside the cell means that cheaper materials can be used. For the case with hydrocarbon fuel the temperature decreases as the methane is catalytically reformed.

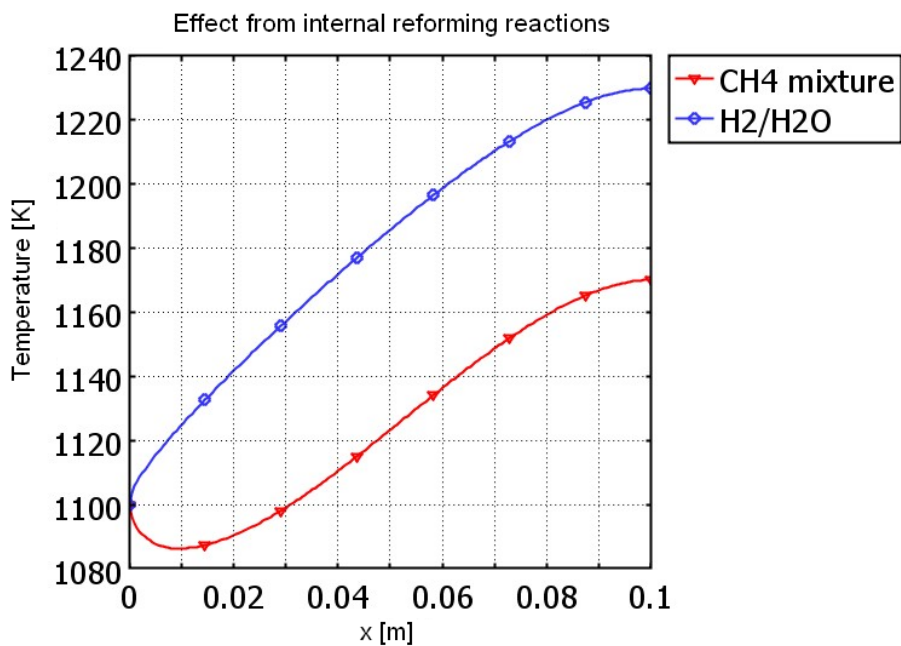


Figure 25: Gas phase temperature within the fuel channel.

Chapter 5

Conclusions

SOFCs can be described at different length- and time scales. A challenge faced is to further develop multiscale models for fuel cell designs. The multiscale models can provide a clear understanding of operating conditions, transport and reaction phenomena at the microscale connected to, e.g., conditions in the air and fuel channels at the macroscale. It is possible to couple different physical models, for example models at the microscale describing transport phenomena inside an anode with a macroscale model describing the entire fuel cell. Use of multiscale modeling in fuel cell research will lead to an increased power density and also to a decreased cost for development and production, and an increased energy efficiency, i.e., the commercialization of fuel cells will be promoted.

In this study, a CFD approach is developed and implemented to analyze physical phenomena that take place inside an anode-supported SOFC. Equations for heat-, mass- and momentum transport are solved simultaneously. An LTNE approach is applied to calculate the temperatures in the solid phase and gas phase separately. It is concluded that the temperature difference between the gas and solid phases is negligible for the investigated conditions. It is found that activation polarization for both the anode and cathode as well as ohmic polarization in the electrolyte cause a significant effect on the temperature in the intermediate temperature range. An increased inlet temperature decreases the polarization losses within the cell, however an increased operation temperature requires more expensive materials. The ionic conductivity in the electrolyte can be increased with advanced material or design. It is found that changing the oxygen surplus factor is an easy approach to control the temperature increase within the cell. It is important for the counter flow design to keep the inlet temperature of the fuel stream close to the outlet temperature of the air stream, to avoid too high temperature gradients close to the fuel flow inlet.

The temperature within the cell decreases as a methane rich fuel is used. A decreased temperature means that cheaper construction materials can be used. The reforming reaction rate depends strongly on temperature. Consumption of hydrogen and production of water at the anodic TPB along the flow direction makes the water-gas shift reaction to proceed to the right (and produce more hydrogen). For this study around 45 % of the heat generated can be used by the steam reforming reaction. This increases the cell efficiency.

Chapter 6

Future work

The fuel cell is not a new invention, the principle dates back to 1838. However, the fuel cell technology is approaching the commercial phase, the potential for the future is enormous and fuel cells can be a key component in a future sustainable energy system. To achieve this big importance the production cost must be decreased and the life length must be increased. One way to decrease the operating temperature and also increase the life time is to increase the understanding of multiscale transport- and reaction phenomena within the cell.

Fuel cell operation depends on complex interaction between multi-physics such as fluid flow, mass and heat transfer and (electro-) chemical reactions. Coupling of these phenomena, i.e., multiscale modeling, is promising for future fuel cell research. Micro- and macroscale physical phenomena and chemical reactions could be solved together.

The ionic transport in the electrolyte as well as detailed TPB shape has not been considered so far. Since the ohmic polarization in the electrolyte cause a significant part of the heat losses within the cell, this should be included and considered in future extended models. Besides the ohmic polarization in the electrolyte, the activation potential in the electrodes causes also a big part of the heat losses. More knowledge and understanding of the effect behind the activation is important to enable reduction of the operating temperature.

The basic model, described in this thesis, considers hydrogen and water on the fuel side. The extended model covers hydrogen, water, methane, carbon monoxide and carbon dioxide. It would be interesting to study more advanced fuel mixtures such as natural-gas and bio-gas, and hydrocarbons with longer coal chains as well. It should be mentioned that natural-gas consists of a mixture of several different gas species, and the composition varies depending on geographical origin.

The model described in this thesis does not consider the Knudsen diffusion, which describes collisions between the gas molecules and the porous structure (inside the porous electrodes), Instead the Stefan-Maxwell diffusion approach is implemented, which considers the collisions between the gas molecules only. Implementation of the Knudsen diffusion will increase accuracy for the mass transport calculation in the electrodes, particularly with big current densities.

The reforming reaction rate is dependent on temperature, concentrations, type and catalyst available. It is expected that a model considering catalytic chemical surface reactions (instead of global kinetics expressions used in this thesis) will be valuable for future fuel cell development.

The work in this thesis includes phenomena on the cell level only. A scale-up to stack and further to system level will be of interest for investigations.

The modeling so far relies on the governing equations of heat, mass and momentum transport. Physical and material properties are calculated from data found in literature. Experimental work is desired for validation of the model.

Chapter 7

References

- [1] Li P.-W. , Schaefer L., Chyu M.K., Multiple transport processes in solid oxide fuel cells, Chapter 1 in Sundén B., Faghri. M., Transport Phenomena in Fuel Cells, WIT Press, UK, 2005
- [2] Yuan J., Faghri M., Sundén B., On heat and mass transfer phenomena in PEMFC and SOFC and modelling approaches, Chapter 4 in Sundén B., Faghri. M., Transport Phenomena in Fuel Cells, WIT Press, UK, 2005
- [3] Fuel Cell Handbook (the seventh edition), EG&G Technical Services Inc., U.S. Department of Energy, Morgantown, Virginia, USA, 2004
- [4] Saxe M., Bringing fuel cells to reality and reality to fuel cells, Doctoral thesis, Department of Chemical Sciences and Engineering, KTH- Royal Institute of Technology, Sweden, 2008
- [5] Kemm M., Dynamic Solid Oxide Fuel Cell Modelling for Non-steady State Simulation of System Applications, Doctoral thesis, Department of Energy Sciences, Lund University, Sweden, 2006
- [6] Chen E., History, Chapter 2 in Hoogers G., Fuel Cell Technology Handbook, CRC Press LLC, USA, 2003
- [7] Aicher T., Lenz B., Gschnell F., Groos U., Federici F., Caprile L., Parodi, Fuel processors for fuel cell APU applications, *J. Power Sources*, **154**, pp. 503-508, 2006
- [8] Cutillo A., Specchia S., Antonini M., Saracco G., Specchia V., Diesel fuel processor for PEM fuel cells: Two possible alternatives (ATR versus SR), *J. Power Sources*, **154**, pp. 379-385, 2006
- [9] Prospects for hydrogen and fuel cells, International Energy Agency, Paris, France, 2005
- [10] Zhu H., Kee R., Janardhanan V., Deutschmann O., Goodwin D., Modeling Elementary Heterogeneous Chemistry and Electrochemistry in Solid-Oxide Fuel Cells, *J. Electrochem. Soc.*, **152**, pp. A2427-A2440, 2005
- [11] Gooenough J.B., Huang Y., Alternative Anode Materials for Solid Oxide Fuel Cells, *J. Power Sources*, **173**, pp. 1-10, 2007
- [12] Ni M., Leung M.K.H., Leung D.Y.C., Micro-Scale Modeling of Solid Oxide Fuel Cells with Micro-structurally Grades Electrodes, *J. Power Sources*, **168**, pp. 369-378, 2007
- [13] Bessler W.G., Gewies S., Vogler M., A New Framework for Physically Based Modeling of Solid Oxide Fuel Cells, *Electrochim. Acta*, **53**, pp. 1782-1800, 2007
- [14] Janardhanan V., Deutschmann O., CFD Analysis of a Solid Oxide Fuel Cell with Internal Reforming, *J. Power Sources*, **162**, pp. 1192-1202, 2006

-
- [15] Hecht E., Gupta G., Zhu H., Dean A., Kee R., Maier L., Deutschmann O., Methane reforming kinetics within a Ni-YSZ SOFC anode support, *Applied Catalysis A : General*, **295**, pp. 40-51, 2005
- [16] Kackac S., Pramuanjaroenkij A., Zhou X., A Review of Numerical Modeling of Solid Oxide Fuel Cells, *I. J. Hydrogen Energy*, **32**, pp. 761-786, 2007
- [17] Yakabe H., Ogiwara T., Hishinuma M. Yasuda I., 3-D model calculation for planar SOFC, *J. Power Sources*, **102**, pp. 144-154, 2001
- [18] Kumar V., Arora A., Pandey O.P., Singh K., Studies on thermal and structural properties of glasses as sealants for solid oxide fuel cells, *Int. J. Hydrogen Energy*, **33**, pp. 434-438, 2008
- [19] Suzuki K., Iwai H., Nishino T., Electrochemical and thermo-fluid modelling of a tubular solid oxide fuel cell with accompanying indirect internal fuel reforming, Chapter 3 in Sundén B. et. al. Transport Phenomena in Fuel Cells, WIT Press, UK, 2005
- [20] Klein J.-M., Bultel Y., Pons M., Ozil P., Current and voltage distributions in a tubular solid oxide fuel cell (SOFC), *J. Applied Electrochemistry*, **38**, pp. 497-505, 2008
- [21] Huang Y., Ningbo Institute of Materials Technology and Engineering (NIMTE), Chinese Academy of Science (CAS), e-mail communication 2009-03-17
- [22] Liu Q.L., Khor K.A., Chan S.H., High performance low-temperature solid oxide fuel cell with novel BSCF cathode, *J. Power Sources*, **161**, pp. 123-128, 2006
- [23] Suzuki T., Yamaguchi T., Fujishiro Y., Awano M., Fabrication and characterization of micro tubular SOFCs for operation in the intermediate temperature, *J. Power Sources*, **160**, pp. 73-77, 2006
- [24] Inagaki T., Nishiwaki F., Knaou J., Yamasaki S., Hosoi K., Miyazawa T., Yamanda M., Komada N., Demonstration of high efficiency intermediate-temperature solid oxide fuel cell based on lanthanum gallate electrolyte, *J. Alloys and Compounds*, **408-412**, pp. 512-517, 2006
- [25] Young D., Computational Chemistry A Practical Guide for Applying Techniques to Real-World Problems, John Wiley & Sons, USA, 2001
- [26] Karakasidis T., Charitidis C., Multiscale Modelling in Nanomaterials Science, *Mater. Sci. Eng.*, **C27**, pp. 1082-1089, 2007
- [27] Frayret C., Villesuzanne A., Pouchard M., Matar S., Density Functional Theory Calculations on Microscopic Aspects of Oxygen Diffusion in Ceria-Based Materials, *I. J. Quantum Chemistry*, **101**, pp. 826-839, 2005
- [28] Cheng C.H., Chang Y.W., Hong C.W., Multiscale Parametric Studies on the Transport Phenomenon of a Solid Oxide Fuel Cell, *J. Fuel Cell Sci. Technol.*, **2**, pp. 219-225, 2005
- [29] Modak A.U., Lusk M.T., Kinetic Monte Carlo Simulation of a Solid-oxide Fuel Cell, *Solid State Ionics*, **176**, pp. 1281-1291, 2005
- [30] Joshi A.S., Grew K.N., Peracchio A.A., Chiu W.K.S., Lattice Boltzmann Modeling of 2D Gas Transport in a Solid Oxide Fuel Cell Anode, *J. Power Sources*, **164**, pp. 631-638, 2007
- [31] Suwanwarangkul R., Croiset E., Fowler M.W., Douglas P.L., Entchev E., Douglas M.A., Performance Comparison of Fick's, Dusty-gas and Stefan-Maxwell Models to Predict the Concentration Overpotential of a SOFC Anode, *J. Power Sources*, **122**, pp. 9-18, 2003
- [32] Ni M., Leung M.K.H., Leung D.Y.C., Micro-Scale Modeling of a Functionally Graded Ni-YSZ Anode, *Chem. Eng. Technol.*, **30**, pp. 287-592, 2007

-
- [33] Park J., Li X., Multi-phase micro-scale flow simulation in the electrodes of a PEM fuel cell by lattice Boltzmann method, *J. Power Sources*, **178**, pp. 248-257, 2008
- [34] Deshmukh S.R., Mhadeshwar A.B., Lebedeva M.I., Vlachos D.G., From Density Functional Theory to Microchemical Device Homogenization: Model Prediction of Hydrogen Production for Portable Fuel Cells, *Int. J. Multiscale Comp. Eng.*, **2**, pp. 221-238, 2004
- [35] Yuan J., Ren F., Sunden B., Analysis of Chemically Reacting Transport Phenomena in an Anode Duct of Intermediate Temperature SOFCs, *J. Fuel Cell Sci. Technol.*, **3**, pp. 687-701, 2006
- [36] Huang W., Huang X., Reifsnider K., Meso-Scale Multiphysics Model of SOFC Cathode Processes, *COMSOL Users Conference Boston*, 2006
- [37] Versteeg H.K., Malalasekera W, An Introduction to Computational Fluid Dynamics, The Finite Volume Method, Pearson, UK, 1995
- [38] Pasaogullari U., Wang C.-Y., Computational Fluid Dynamics Modeling of Solid Oxide Fuel Cells, Proceedings of SOFC-VIII, Eds. S.C. Singhal and M. Dokiya, pp. 1403-1412, 2003
- [39] Autissier N., Larrain D., van Herle J., Favrat D., CFD Simulation Tool for Solid Oxide Fuel Cells, *J. Power Sources*, **131**, pp. 131-319, 2004
- [40] Hussein M.M., Li X., Dincer I., Mathematical Modeling of Transport Phenomena in Porous SOFC Anodes, *Int. J. Thermal Sciences*, **46**, pp. 48-86, 2007
- [41] Dennis, B.H., Han Z., Jin W., Wang B.P., Xu L., Aapro, T., Ptchelintsev, A., Reinikainen T., Multi-Physics Simulation Strategies with Application to Fuel Cell Modeling, 7th. Int. Conf. on Thermal, Mechanical and Multiphysics Simulation and Experiments in Micro-Electronics and Micro-Systems, EuroSimE, 2006
- [42] Reifsnider K., Huang X., Ju G., Solasi R., Multi-scale Modeling Approaches for Functional Nano-composite Materials, *J. Mater. Sci.*, **41**, pp. 6751-6759, 2006
- [43] Tseronis K., Kookos I., Theodoropoulos K., Modelling and Design of the Solid Oxide Fuel Cell Anode, *COMSOL Users Conference Birmingham*, 2006
- [44] Nam J.H., Jeon D.H., A Comprehensive Micro-scale Model for Transport and Reaction in Intermediate Temperature Solid Oxide Fuel Cells, *Electrochim. Acta*, **51**, pp. 3446-3460, 2006
- [45] Haile S.M., Fuel Cell Materials and Components, *Acta Mater.*, **51**, pp. 1981-2000, 2003
- [46] Pramuanjaroenkij A., Kakac S., Zhou X. Y., Mathematical analysis of planar solid oxide fuel cells, *Int. J. Hydrogen Energy*, **33**, pp. 2547-2565, 2008
- [47] Ivanov P., Thermodynamic modeling of the power plant based on the SOFC with internal steam reforming of methane, *Electrochimica Acta*, **52**, pp. 3921-3928, 2007
- [48] Lee W.Y., Wee D., Ghoniem A.F., An improved one-dimensional membrane-electrolyte assembly model to predict the performance of solid oxide fuel cell including the limiting current density, *J. Power Sources*, **186**, pp. 417-427, 2009
- [49] Haberman B.A., Young J.B, Three-dimensional simulation of chemically reacting gas flows in the porous support structure of an integrated-planar solid oxide fuel cell, *Int. J. Heat and Mass Transfer*, **47**, pp. 3617-3629, 2004
- [50] Chan, S.H., Khor K.A., Xia Z.T., A Complete Polarization Model of a Solid Oxide Fuel Cell and its Sensitivity to Change of Cell Component Thickness, *J. Power Sources*, **93**, pp. 130-140, 2001

-
- [51] Yuan J., Huang Y., Sundén B., Wang W.G., Analysis of parameter effects on chemical coupled transport phenomena in SOFC anodes, *Heat Mass Transfer*, **45**, pp. 471-484, 2009
- [52] Hyun N. J., Hyup J. D., A comprehensive micro-scale model for transport and reaction in intermediate temperature solid oxide fuel cells, *Electrochimica Acta*, **51**, pp. 3446-3460, 2006
- [53] Bove R., Ubertini S., Modeling Solid Oxide Fuel Cell Operation: Approaches, Techniques and Results, *J. Power Sources*, **159**, pp. 543-559, 2006
- [54] Le Bars M., Grae Worster, M., Interfacial Conditions Between a Pure Fluid and a Porous Medium, Implications for Binary Alloy Solidification, *J. Fluid Mech.*, **550**, pp.149-173, 2006
- [55] Lister S., Djilali N., Two-phase transport in porous gas diffusion electrodes, Chapter 5 in Sundén B., Faghri. M. Transport Phenomena in Fuel Cells, WIT Press, UK, 2005
- [56] Boder M., Dittmeyer R., Catalytic modification of conventional SOFC anodes with a view to reducing their activity for direct internal reforming of naturalgas, *J. Power Sources*, **155**, pp. 13-22, 2006
- [57] Damm D.L., Fedorov A.G., Local Thermal Non-Equilibrium Effects in Porous Electrodes of the Hydrogen Fueled SOFC, *J. Power Sources*, **159**, pp. 1153-1157, 2006
- [58] Janardhanan V.M., Deutschmann O., Numerical Study of Mass and Heat Transport in Solid-Oxide Fuel Cells Running on Humidified Methane, *Chem. Eng. Sci.*, **62**, pp. 5473-5486, 2007
- [59] Barzi Y.M., Ghassemi M., Hamed M.H., Afshari E., Numerical Analysis of Output Characteristics of a Tubular SOFC with Different Fuel Compositions and Mass Flow Rates. In: Proceedings of *Solid Oxide Fuel Cells 10 (SOFCX)*, Eguchi, K., Singhal, S.C., Yokokawa, H. and Mizusaki, J. (eds.). ECS Transactions, **7**, pp. 1919-1928, 2007
- [60] Aguiar P., Adjiman C.S., Brandon N.P., Anode-supported intermediate-temperature direct internal reforming solid oxide fuel cell II. Model-based dynamic performance and control, *J. Power Sources*, **147**, pp.136-147, 2005
- [61] King D., Strohm J., Wang X., Roh H.-S., Wang C., Chin Y.-H., Wang Y., Lin Y., Rozmiarek R., Singh P., Effect on nickel microstructure on methane steam reforming activity of Ni-YSZ cermet anode catalyst, *J. Catalysis*, **258**, pp. 356-365, 2008
- [62] Molenda J., Swierczek K., Zajac W., Functional materials for IT-SOFC, *J. Power Sources*, **173**, pp. 657-670, 2007
- [63] Rosterup-Nielsen J.R., Hansen J.B., Helveg S., Christiansen N., Jannasch A.-K., Sites for catalysis and electrochemistry in solid oxide fuel cell (SOFC) anode, *Appl. Phys.*, **A85**, pp. 427-430, 2006
- [64] Clarke S., Dicks A., Pointon K., Smith T., Swann A., Catalytic aspects of the steam reforming of hydrocarbons in internal reforming fuel cells, *Catalysis Today*, **38**, pp. 411-423, 1997
- [65] Janardhanan V., Deutschmann O., CFD analysis of a solid oxide fuel cell with internal reforming: Coupled interactions of transport, heterogeneous catalysis and electrochemical processes, *J. Power Sources*, **162**, pp. 1192-1202, 2006
- [66] Wang L., Zhang H., Weng S., Modeling and simulation of solid oxide fuel cell based on the volume-resistance characteristic modeling technique, *J. Power Sources*, **177**, pp. 579-589, 2008

-
- [67] Nagel F., Schildhauer T., Biollaz S., Stucki S., Charge, mass and heat transfer interactions in solid oxide fuel cells operated with different fuel gases – A sensitivity analysis, *J. Power Sources*, **184**, pp. 129-142, 2008
- [68] Tseronis K., Kookos I. K., Theodoropoulos C., Modeling mass transport in solid oxide fuel cell anodes: a case for a multidimensional dusty gas-based model, *Chem. Eng. Sci.*, **63**, pp. 5626-5638, 2006
- [69] Lehnert W., Meusinger J., Thom F., Modelling of gas transport phenomena in SOFC anodes, *J. Power Sources*, **87**, pp 57-63, 2000
- [70] Yakabe H., Hisinuma M., Uratani M., Matsuzaki Y., Yasuda I., Evaluation and modeling of performance of anode-supported solid oxide fuel cell, *J. Power Sources*, **86**, pp. 423-431, 2000
- [71] Ferguson J.R., Fiard J.M., Herbin R., Three Dimensional Numerical Simulation for Various Geometries of Solid Oxide Fuel Cells, *J. Power Sources*, **58**, pp. 109-122, 1996
- [72] Aguiar P., Adjiman C.S., Brandon N.P., Anode-supported intermediate temperature direct internal reforming solid oxide fuel cell. I: model-based steady-state performance, *J. Power Sources*, **138**, pp.120-136, 2004
- [73] COMSOL Multiphysics 3.5 user guide, Stockholm, Sweden, 2008
- [74] Todd B., Young J.B., Thermodynamic and Transport Properties of gases for use in Solid Oxide Fuel Cell Modeling, *J. Power Sources*, **110**, pp. 186-200, 2002
- [75] Nordelöf A., Salsing C., SOFC Modeling in FEMLAB, Master thesis, Chalmers University, Sweden, 2003
- [76] Reid R.C., Prausnitz J.M., Poling B.E., The Properties of Gases & Liquids, Fourth edition, R.R. Donnelley & Sons Company, USA, 1986
- [77] Chao C.H., Hwang A.J.J., Predictions of Phase Temperatures in a Porous Cathode of Polymer Electrolyte Fuel Cells using a Two-Equation Model, *J. Power Sources*, **160**, pp. 1122-1130, 2006
- [78] Marrero-López D., Ruiz-Morales J.C. Peña-Martínez J., Canales-Vázquez J., Núñez P., Preparation of Thin Layer Material with Macroporous Microstructure for SOFC Applications, *J. Solid State Chemistry*, **181**, pp. 685-692, 2008
- [79] Chan S.H., Low C.F., Ding O.L., Energy and Exergy Analysis of Simple Solid-Oxide Fuel-Cell Power Systems, *J. Power Sources*, **103**, pp. 188-200, 2002
- [80] Shah R.K., London A.L., Laminar Flow Forced Convection in Ducts. Academic Press, London, UK, 1978
- [81] Bessler W.G., Warnatz J., Goodwin D.G., The Influence of Equilibrium Potential on the Hydrogen Oxidation Kinetics of SOFC anodes, *Solid State Ionics*, **177**, pp. 3371-3383, 2007
- [82] Ferguson J.R., Fiard J.M., Herbin R., Three-dimensional Numerical Simulation for Various Geometries of Solid Oxide Fuel Cells. *J. Power Sources*, **58**, pp. 109-122, 1996
- [83] Klein J.-M., Bultel Y., Georges S., Pons M., Modeling of a SOFC fuelled by methane: From direct internal reforming to gradual internal reforming, *Chem. Eng. Sci.*, **62**, pp. 1636-1649, 2007
- [84] Sanchez D., Chacartegui R., Munoz A., Sanchez T., On the effect of methane internal reforming in solid oxide fuel cells, *Int. J. Hydrogen Energy*, **33**, pp. 1834-1844, 2008